Investigation of growth process conditions on the nanostructure and interfaces in multilayer coatings for dichroic mirror applications

Written by: Mr David Enyi

URN: 6321904

BEng Aerospace Engineering

Department of Mechanical Engineering Sciences

Faculty of Engineering and Physical Sciences

University of Surrey

Project Report

May 2018

Project Supervisor: Dr Mark Baker

DECLARATION OF ORIGINALITY

I confirm that the submitted work is my own work. No element has been previously submitted for assessment, or where it has, it has been correctly referenced. I have also clearly identified and fully acknowledged all material that is entitled to be attributed to others (whether published or unpublished) using the referencing system set out in the programme handbook. I agree that the University may submit my work to means of checking this, such as the plagiarism detection service Turnitin® UK. I confirm that I understand that assessed work that has been shown to have been plagiarised will be penalised.

David Ogaba Enyi

ABSTRACT

The performance of dichroic mirrors are resolutely dependant on the wavelength of light being used, the optical properties of the metal film and the bilayer and total thickness of the film. In the present work multilayer films were grown on glass and silicon substrates using high intensity target utilization sputtering. In recent years, there has been increase in the use of optical systems in non-visual regions of the electromagnetic spectrum. This surge in the interest in optical coatings, particularly, the multilayers has triggered a need to optimize the transmission and reflective properties of the films. Hence, this report evaluated the performance of cold dichroic mirrors, with characteristic high reflectance in the visible region of the electromagnetic spectrum and high transmission in the infrared and near infrared regions of the spectrum.

The samples were prepared and metallically polished to warrant visualization of the cross section in the SEM, it appears that the layer thicknesses measured show good correlation with the manufacturer's design data, this result is subject to the level of accuracy and resolution attainable on the SEM. Furthermore XPS, FE-SEM, XRD, AFM and optical reflectivity were used to characterise the optical filters, the key results follow that the multilayer films are stoichiometric regardless of thickness of the stack and high reflectance in the visible region is achieved. The drop in transmission observed by PQL is suspected to be a result of the quarter wave stack design and is intrinsic to the behaviour of that particular optical filter. However the trend observed by PQL is consistent outside the zone of high reflection

XPS depth profiles results show consistent stoichiometry across the 7, 11 and 15 layers, additional the depth profiles reveal the same amount of preferential sputtering. However, it must be noted that the clustered ion beam depth profile shows less preferential sputtering in comparison to the monatomic measurements. The peak fitting revealed that only two oxidation states are contributing to the niobium doublet investigated, these are Nb^{5+} and Nb^{5+} confer with data in the literature.

AFM peak force tapping analysis revealed an increase in the surface roughness of the 7, 11 and 15 layer samples and this appears to agree with the diffused reflectance measurements which indicate that unintended scatter is correlated with surface roughness. An attempt has been made to gain a better understanding of the roughness evolution form the substrate to the top of the multilayer stack. It appears that this investigation follows the general trend of periodic oscillatory interface roughening and smoothening obtained during growth of amorphous films. However, more analysis is required to solidify the hypothesis and better understanding of the kinetics of growth may facilitate buttressing the theory.

In summary the research has demonstrated via the composition analysis of the 7, 11 and 15 agrees with the fact that there is no fluctuation of transmission within the high reflectance zone for the multilayers investigated via specular and diffused reflectance. On the other hand diffused reflectance measurements show similar trend to the surface roughness measurements.

ACKNOWLEDGEMENTS

It has indeed been an interesting prospect working in connection with multilayer films and state of the art characterisation methods. However, after a year of learning about multilayer growth and how best to characterize them, I have realised that it is a larger interconnection of fields in physics with a vast array of applications in technological advances.

Considering the fact that I was an alien to the field of materials characterization and multilayer growth, it has truly been a wonderful period of enlightenment and steep learning curved which I have thoroughly enjoyed.

With that said and done I would like to convey my sincere thanks and gratitude to Dr. Mark Baker for his significant contribution in giving guidance throughout this investigation, I'd like to commend his admirable character and dedication to the cause at all times during the year and would like to let him know he is looked upon as a role model in the way he carries himself in his work.

I would also like to thank Dr. Steve Hinder and Dr. Steve Downes for conducting the XPS and Optical Reflectivity experiments respectively. Dr. David Jones and my colleague Alex (Professional Training Year MSSU) for assisting in the SEM experimentation. Furthermore I would like to convey my appreciation to Dr. Harley Brown, Dr. James Dutson and Dr. Steve Wakeham of Plasma Quest Limited for providing supportive information, technical resources and advice whenever I needed it. They have also been cordial and shown great hospitality on my visits to the facility.

A Special thanks to my family for providing the opportunity to me in pursuing the degree, I promise and make it my ultimate duty to repay your efforts and all the blood sweat and tears that you have had to deal with to keep me educated will be compensated with the

I have also been fortunate to have some of the best supportive friends, Khadija Abbas, Kristian Christodoulides, Angga Adi, and to everyone else that have been part of my life for the support throughout the various phases of the project.

Lastly, I would like to express my gratitude to the Big Guy Upstairs, for ultimately steering me down this path. I had no clue where this journey would end when it started and I definitely don't know where it's going from this point, however, I am rest assured that you've got my back in the years to come.

Contents

NOMENCLATURE

Abbreviation	Definition
$(n_L/n_H)^2$	Low refractive index layer / high refractive index layer
2D	Two dimensional
3D	Three dimensional
AES	Auger Electron Spectroscopy
AFM	Atomic Force Microscopy
$Al_{K\alpha}$	Monochromatic Aluminium K-alpha X-rays
Ar^+	Argon Monatomic ion beam
$Ar_{150}+$	Argon cluster ion beam
β	Growth exponent
C1s	Primary XPS region - Carbon
Cu K-alpha	Copper
DC	Direct Current
EDS	Electron Dispersive Spectroscopy
EDXA	Energy Dispersive X-ray Analysis
FE-SEM	Field Emission- Scanning Electron Microscope
FTIR	Fourier Transform Infrared Spectroscopy
FWHM	Full Width at Half Maximum
GCIB	Gas Cluster ion Beam Source
GIXRD	Grazing Incidence Angle Diffraction
HiTUS	High Intensity Target Utilization
L/G_{mix}	Gaussian/Lorentzian ratio
MSSU	Micro-Structural Studies Unit
NASA	National Aeronautics and Space Administration
Nb	Niobium
Nb_2O_5	Niobium pentoxide
Nb3d	Primary XPS region – Niobium
01s	Primary XPS region - Oxygen
PBG	Photonic Band Gaps
PQL	Plasma Quest Limited
PSD	Power Spectral density
PVD	Physical Vapour deposition
PTFE	Polytetrafluorethylene
Ta_2O_5	Tantalum pentoxide
t	Deposition time
RF	Radio frequency
RMS	Root Mean Square Roughness
SEM	Scanning Electron Microscopy
Si	Silicon
Si2p	Primary XPS region – Silicon
Si_3N_4	Silicon Nitride
SIMS	Secondary Ion Mass Spectroscopy
SiO_2	Silicon dioxide
TEM	Transmission electron Microscopy
XPS	X-Ray Photoelectron Spectroscopy
XRD	X-Ray diffraction

1 INTRODUCTION

1.1 Scope

Thin film optical filters possess the ability to demonstrate selective wavelength-dependent transmission or reflectance depending on the desired application. Several forms of optical filters exist and they all feature in a broad spectrum of applications ranging from aircraft cockpit instrumentation to medical photonics. In most of these applications, metal films and metal oxides are often deposited in nanometre scale thicknesses on ceramic substrates and they tend to serve as material with high-quality broadband mirrored surfaces. Interestingly in the 1950s, the first dichroic filters were developed by NASA to protect spacecraft against harmful cosmic radiation, these mirrors can be enhanced to improve the versatility of spectral control in optical microscopy and show promising characteristics for improvements in adaptive optical wave front control. The figure below provides an analogy of how the particular dichroic mirror investigated in this project are employed to achieve reduction in the temperature load of a light source

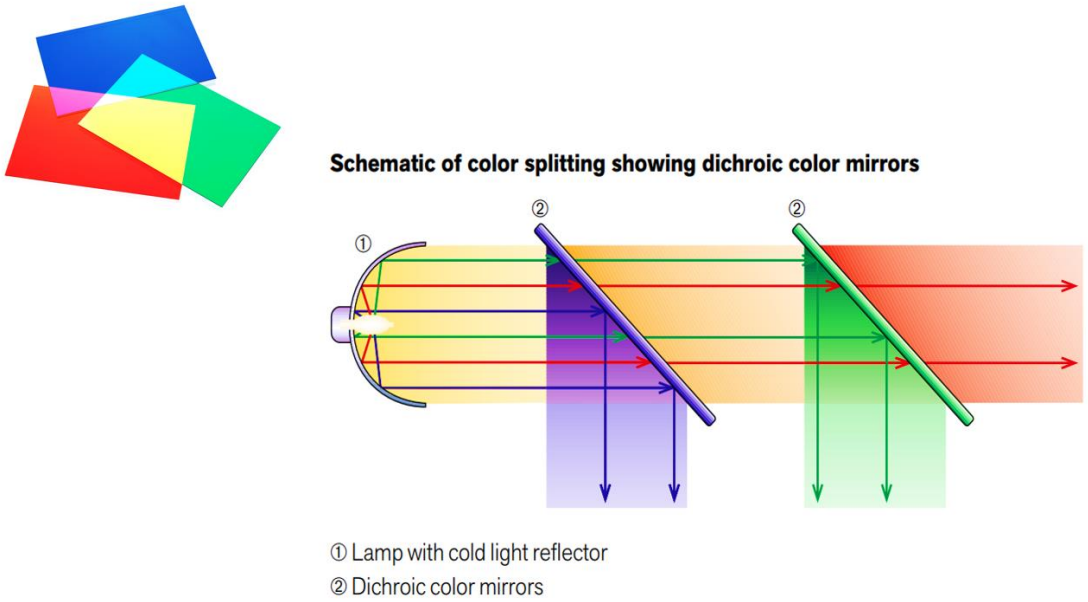

Figure 1: Schematic of application of dichroic mirror in colour separation (Opticsbalzers.com, 2018).

Dichroic mirrors are examples of interference based filters and the samples investigated in this report are quarter wave stack reflectors. The dichroic mirror design studied in this project are referred to as symmetrical periodic multilayers because each half is a mirror image of the other half, this is otherwise referred to as a symmetrical period. Dichroic mirrors are designed to meet very narrow spectral band edge tolerances, high degree of spectral equilibrium and very low residual optical absorption loss. They consist of alternating layers of high-and-low refractive index metal oxide films which are known to be transparent dielectric materials. Light reflected within the high index layers is not susceptible to any phase shift on reflection, low-index-layers on the other hand experience a phase change of $180°$. In this project, the thin films investigated consist of alternating silicon dioxide (SiO_2) commonly known as silica and niobium pentoxide (Nb_2O_5) deposited on glass and silicon substrates. The dielectric materials used in the stack have low optical absorption coefficients to facilitate minimization of energy absorption. Notably, maximum reflectance for a given number of layers is usually obtained with the highest index material as the outermost layer. At the principal wavelengths, constructive interference of the multiple reflected rays

maximizes the overall reflection of the coating, on the other hand, destructive interference among the transmitted rays minimizes the overall transmission. In this regard, the filter characteristics in terms of reflection should complement the characteristics in transmission. As a result, it is expected that the reflectance remains consistently high over a designated range of wavelengths and in regions outside designated wavelengths the reflectance should drop abruptly.
Plasma Quest Limited is a company based in Hook, United Kingdom. They are specialist in the deposition of a wide range of thin films appropriate for use in optical filters using their patented High Intensity Target Utilization (HiTUS) thin film sputter deposition apparatus. The manufacturers have supplied three multilayer samples deposited on substrates of silicon and glass for optical characterization. The major novelty and benefit of HiTUS is that a remotely plasma is generated which offers advantages over conventional sputtering and provides higher efficiency in terms of target erosion due to the uniformity of the plasma. The system also permits the deposition of high quality metal oxide thin films unto flexible substrates by reactive sputtering. The three samples deposited at PQL and used in this project included; 7, 11, and 15-layers of periodic bilayers consisting of all dielectric coating comprising of (SiO_2) and (Nb_2O_5). The work performed with regards to characterizing the microstructure and interfaces of the multilayer samples provided by PQL include; an assessment of uniformity in thickness, a determination of the RMS roughness at the surfaces and the interfaces, an assessment of reflectivity and transmissivity and lastly an evaluation of the atomic composition of the constituent elements in the stack considering their resultant contribution to roughness at reacted zones.

1.2 Problem

Dichroic mirrors are designed to possess the ability to improve reflectivity for a desired wavelength range, various optical components and mirrors can combine these dichroic mirrors to make more efficient systems which operate with less components which necessitate the need requiring for frequent maintenance, also the miniaturization of electronic devices driven by Moore's law makes optical coatings like dichroic mirrors highly sought after. Modern sputtering techniques such as the HiTUS are able to manufacture dense dielectric films with excellent optical and mechanical stability. The deposition technology manufactured by PQL permits accurate deposition of optical filters comprising of multi-layer stacks. The HiTUS system uses a multiple-target holder which provides the capability to repeatedly and reliably deposit identical alternating layers of differing materials, without having to break the vacuum. The major issue addressed in this project with regards to the deposited samples to be examined is related to the loss of transmission observed with the addition of more layers or the increase of the thickness of the multilayer stack. It is suspected that the observed effect is strongly correlated to interface and surface roughness. Subsequently, a review of the literature reveals a more in depth evaluation of the suspected probable causes of the loss in transmission of the films as it relates to the performance of the multilayer films investigated.

1.3 Project Aim & Objectives

The overall aim of this project centres on an investigation into the growth process conditions in the microstructure of dichroic mirrors with quarter wave stack design. Consequently the influence of increasing the number of layers in the stack shall be studied to understand how these conditions adversely affect the transmission of the multilayer samples via several experimental procedures. The interfaces in these mirrors are particularly of interest, thus, emphasis has been laid on this area to enable visualization and quantification of optical performance in the samples investigated. This has been undertaken by considering by considering four key aspects; (a) Determination of topography and morphology of the samples, (b) Determination of atomic composition of the constituent elements in multilayer stack (c)

Determination of Surface and interface roughness and (d) Evaluation of the crystalline or amorphous nature of the samples. Considerations were also made with regards to determination of the interrelationship between optical performance and the increase in number of layers. It is expected that the results obtained from all experiments conducted are utilized to provide more insight into growth conditions during deposition at Plasma Quest Limited, essentially facilitating improvements in process refinement and synthesis.

1.4 Approach

To facilitate the exploration and analysis of the growth conditions in the nanostructure of the dichroic mirror samples and to gain a better understanding of the nature of the microstructure at interfaces, a work plan was drawn out to facilitate traceability and coherence of findings of the project. An overview of the work package as depicted in table 1 consists of five categories. These categories formulate the major objectives set out with the Project supervisor to satisfy the project aims.

Table 1: Outline of the Project plan used for correlation of thin film characterisation and optical performance.

Category	Properties of interest	Techniques employed
Surface Topography measurements	RMS surface roughness	Atomic Force Microscopy
Surface morphology measurements	Atomic composition (%) on surface of material	Scanning Electron Microscopy and Energy Dispersive Spectroscopy.
Cross sectional imaging	Layer thickness estimation	Cross Sectional SEM
Subsurface morphology measurements	Elemental composition as a function of depth	X-Ray Photoelectron Spectroscopy
Determination of reflectivity and transmissivity.	Percentage transmittance and reflectance	Optical Reflectivity
Crystal structure evaluation	Degree of crystallinity & crystal symmetry	X-Ray diffraction

2 LITERATURE REVIEW

2.1 Introduction

The concepts which cumulatively describe the rationale and establish the basis for the methodical investigation of thin multilayer coatings in this project are divided into four sub groups and they collectively formulate the frame of reference for the project developments in terms of the literature survey. A brief account of the history optics has been included to account for the chronological build up to the technology under study. This study on dichroic mirrors essentially fits into the broader spectrum of modern optics due to the significance attached to the application of fully reflective mirrors and neutral density filters in several electronic devices today. A wide variety of filter designs are produced to meet the precise specifications for excellent optimal performance in terms of transmission and reflection. The

themes explored to effectively assess the performance of dichroic mirrors in this project include; Multilayer thin film principles, Interfacial roughening and smoothening, effects of stress on optical performance of multilayers and lastly the techniques of optical and compositional characterization. A diagrammatic illustration of these themes is provided to aid visualization of the scope of the project.

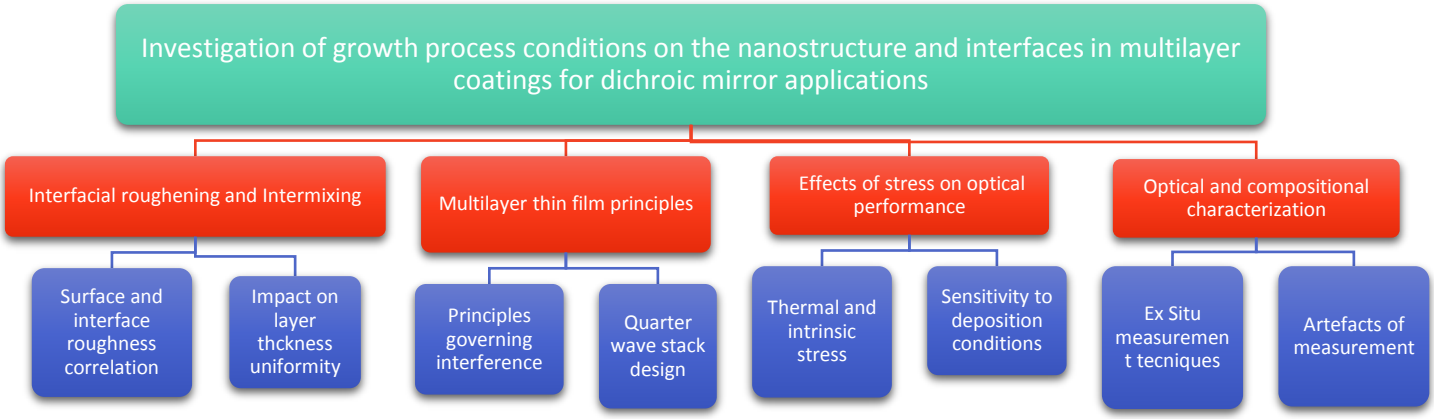

Figure 2: Schematic overview of the of the literature survey.

2.2 Historical Review

The pioneers in the field of what is today regarded as modern thin film optics are Robert Boyle and Robert Hooke, they both independently discovered the phenomenon known a Newton's rings. In 1801, Thomas Young expanded on the principle and produced the first satisfactory explanation of the interference of light. However, the foundation of the theory of light was buttressed in history by Augustin Jean Fresnel via his work in establishing the transverse nature of light and the theory of diffraction. Fresnel's laws governing the phase and amplitude of light reflected and transmitted at a single boundary is of major relevance in thin film construction. Due to Fresnel's collaboration with Simeon Denis Poisson in their elegant piece of work involving transmittance and interference effects, a better understanding of the principle of half waves and quarter waves in relation to reflectance at a surface was developed. In the nineteenth century, developments became far more rapid and a massive growth in the field of interferometry lead to the beginnings of thin -film optical coatings. This rapid growth came about in the 1930's via the advent of manufacturing processes with high fidelity pumping systems such as sputtering and vacuum evaporation. In terms of practicality, the real limitations to what is today achievable in optical thin film filters and coatings is the capability of the manufacturing processes available to produce layers of precisely the correct optical constants and thicknesses (Macleod, 2010).

2.3 Multilayer Thin film Principles

Multilayer thin films are designed to function as interference filters, the fundamental principles governing reflection and transmission of light on a smooth interface between two transparent media are directly related to the interaction of a single thin film or multilayer stack deposited on a highly polished substrate.

Reflection of incident light at an air glass interface plays a significant role in optical devices, as such it follows that thickness and refractive index of layers in a stack are alternated by design to control transmission and reflection at specific wavelengths. Figure 3 below illustrates how the layered structure in thin films are manipulated to generate either constructive or destructive interference by each interface for certain wavelength ranges.

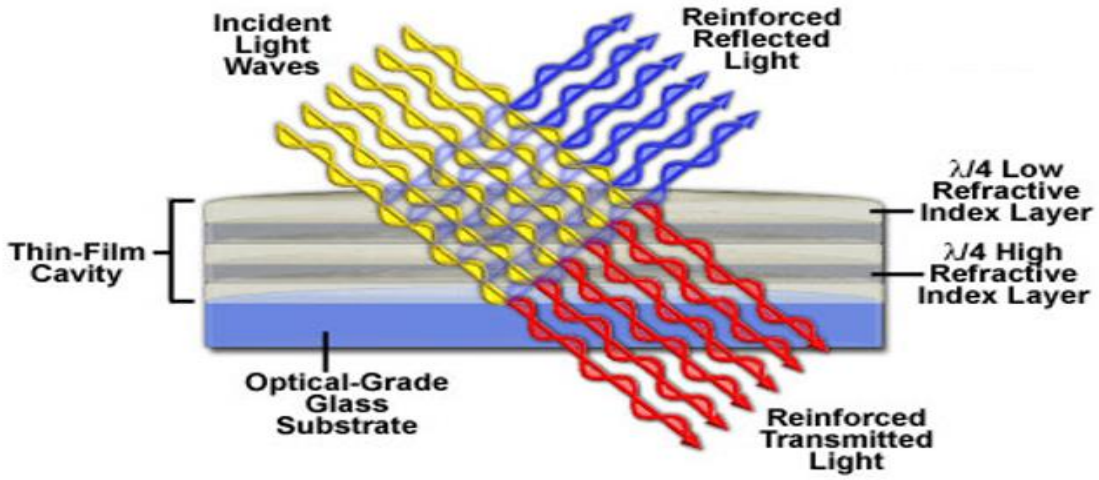

Figure 3: Schematic illustrating reflection and transmission by interference filters (Hardee, 2018)

Quarter wave stack reflector is the underlying principle used as the fundamental building block for a wide range of thin film filters, the two major limitations experienced in their application stem from the underlying adverse effect of variable change in phase associated with reflection and the limited high reflection zone. The design procedure for dichroic mirrors involves a single modified quarter wave reflector, the high and low index layer thicknesses are graded between the quarter wave thicknesses of two wavelengths at either end of the intended broadband performance region. In many scanning dye laser systems, it is imperative to have high reflectance over a large wavelength region. If proper consideration is not taken at the material selection stage to ensure precise variation in refractive index in a multilayer, there is a resultant degrading effect on the optical performance of the filters. From a heuristic perspective, to enhance image quality, materials are selected with the highest degree of homogeneity, the lowest number of inclusions, and the best match in refractive index at the interfaces. To understand the behaviour of a quarter-wave stack it is beneficial to appreciate the concept of high-reflection zone shown in figure 4. This reflection zone is limited in extent and it falls abruptly to low oscillatory values outside designated wavelengths. According to Macleod, the addition of extra layers does not affect the width of the zone of high reflectance, however, it causes a rise in reflectance within the zone and decreases the number of oscillations outside this zone for a given odd number of layers. Notably, (Macleod, 2010) has shown that the transmittance reduces by a factor of $(n_L/n_H)^2$ with the addition of two extra layers, where n_L and n_H represent the high and low refractive indices in the multilayer stack. It follows that the adsorption in these materials is reported to be potentially less than 0.01%, as long as the materials used are transparent. However, Schiffmann and Vergohl have reported in their research that factors such as statistical process variations, variations in optical paths and deviations in instrument alignment contribute to the nonconformity of the film stack from computed theoretical design. Therefore,

ex situ measurements aimed at confirming predefined design layer thicknesses and refractive indices are critical to ascertain the level of quality control required in process refinement and synthesis of existing sputtering technology used in deposition of optical coatings.

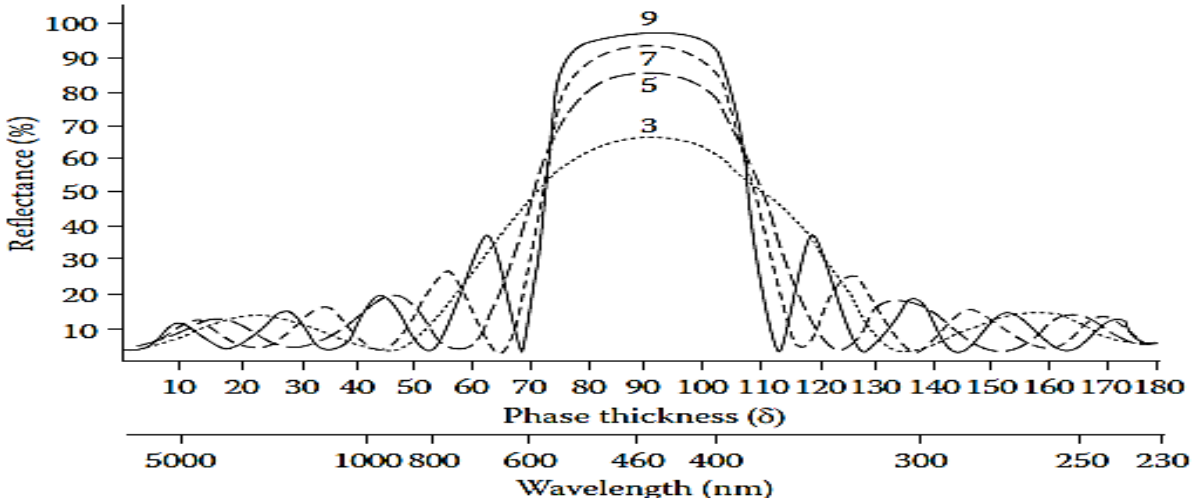

Figure 4: Underlying principle of the quarter wave stack employed in dichroic mirrors (Smith, W. 2000).

2.4 Interfacial roughening & Atomic Mixing

The growth of optical coatings generates interface roughness and checking for this effect during deposition is important, the techniques through which in situ layer thickness measurements are achieved is a crucial element in dichroic mirror production. According to Schiffmann and Vergohl nucleation and growth of coatings gives rise to interface roughness which cannot be accounted for during deposition of thin films. Since the design of dichroic mirrors requires an arrangement which will give a performance specified in advance, it means that the accuracy of each layer thickness in a multilayer stack is crucial. From the work by Gupta et al. it is suggested that during deposition, the roughness of the substrate is partially transmitted to the surface of the film. Additionally, findings by Savage et al., also suggests that interfacial roughness is related to surface roughness because the same kinetic boundaries are present during the growth of an individual layer as in a single film. In ideal interfaces where there is no chemical reaction or inter diffusion between layers, the interfacial roughness at a given layer is simply the surface roughness of the film. Multilayer samples which comprise of two dielectric materials are deposited alternately, the evolution of roughness is correlated as a function of total thickness, bilayer thickness, and thickness ratio between two indexing materials in a stack. The phenomena known as smoothening and roughening exists at alternate interfaces of multilayer samples and has been observed by Paul et al. in experimentation involving a DC magnetron sputtered Platinum-Carbon multilayers. Observations made in research undertaken by Haque and Bhattacharya in the case of ion beam sputter deposited Tungsten-Silicon multilayer samples is in agreement with research carried out by Paul et al.

The overall roughness profile of a multilayer stack has an ultimate dependence on the total number of bilayers, the bilayer period, and the multilayer thickness ratio (Ghafoor, 2005). It has also been suggested by Ghafoor (2005) that the independence of interfacial roughness on the bilayer period yields inefficient

optical reflectors and the roughness at the interface is controlled by the evolution of individual layer morphologies. In other similar experiments, a gradual decrease in interface roughness of Silicon-Tungsten multilayers from the substrate to the top of the multilayer has been observed by Biswas and Bhattacharyya (2011), this follows the trend found by Paul et al. (2002) where evidence of smoothening as the number of layers is increased has been observed and the effect is more visible for multilayers with a higher number of layers in the stack. However this contradicts findings by Schiffmann and Vergohl, which suggest that interface roughness increase from the bottom to the top of the stack.

2.5 Effects of stress on Optical performance

All vacuum deposited coatings are in a state of stress and the total stress in the stack comprises of a thermal and an intrinsic stress and the substrate dictates the behaviour of the multilayer stack under stress (Hoffman and Thornton, 1989). The film-substrate bond in multilayers must be capable of withstanding the force produced by cumulated intrinsic and thermal stresses, if this condition does not hold, subsequent exposure of the substrate to heating or thermal cycles could potentially cause tensile cracking or compressive buckling. The formation of stress controlled reflection layers which perform satisfactorily as micromechanical elements has been investigated by Richter et al (2001), in so doing it was discovered that such multilayers do not perform satisfactorily if the form and profile of the stack is considerably distorted by tensile or compressive forces. Richter reports an observed relationship between stress and bias voltage in sputter deposition of thin films. Referenced sources of stress which can be found in niobium pentoxide and silicon dioxide multilayers include; (a) A rise in compressive stress in Nb_2O_5 which results from increasing substrate biasing temperature and voltage, (b) Slight increase in compressive stress with reduced bias voltage caused due to residual water vapour in SiO_2. Although the compressive stress in a dielectric cannot be fully compensated, it is reported that an underlying tensile layer with a thickness proportional to the weight contribution of SiO_2 and Nb_2O_5 considerably alleviates the stress levels experienced in multilayer stacks. An investigation into the optical and structural properties of Nb_2O_5-SiO_2 mixtures by Janicki et al. (2013) reported that SiO_2 films are amorphous and are intrinsically prone to compressive stress. It is also reported that Nb_2O_5 is amorphous on deposition, even though it possesses the propensity to be crystalline. According to Janicki et al. (2013) the capacity for Nb_2O_5 to form a crystalline phase is dependent on the degree of interaction which occurs with SiO_2 and it is speculated that SiO_2 acts as a stabilizer of Nb_2O_5 by decreasing its mobility level and consequently preventing crystallinity. Furthermore, the sputtering process facilitates the fabrication of amorphous phase as shown in work conducted by Wasa and Hayakawa (1992), and the HiTUS technology reportedly possess the ability to control the growth mechanism of the material, ranging from amorphous to crystalline and also directing the preferred crystalline direction (Plasma Quest, 2018). Essentially, understanding the stresses generated during deposition and the stress profile of PVD manufactured films will be highly beneficial to optimizing the performance of multilayers in their various applications.

2.6 Optical & Compositional Characterization of Multilayers

The rising importance in development of laser technologies has profoundly increased the demand for high-quality optical thin films which possess physical properties that are malleable and well defined (Whiteside, Chininis, and Hunt, 2016). Such films are commonly deposited in thicknesses much shorter than the wavelengths of visible light and consequently present challenges for characterization by traditional microscopy. In thin film design, the optical constants of the material mixture must be calculated to obtain an assessment of the design and its optical performance. Effective medium theories such as the Lorentz – Lorenz are used depending on the material mixture and deposition technique to perform optical

characterization. (Janicki et al., 2012) utilizes the Lorentz-Lorenz effective medium theory in tandem with *ex situ* measurements such as Fourier Transform Infrared Spectroscopy [FTIR], transmission electron Microscopy [TEM], X-Ray diffraction [XRD] and atomic force microscopy [AFM] which are subsequently described in this section to characterize Nb_2O_5. This project follows the same trend with regards to methods used in as the findings in Janicki et al., and reflect similarity in the characterization methods employed (Janicki et al., 2012). The focal methods of surface and interface analysis are Auger Electron Spectroscopy [AES], X-Ray photoelectron Spectroscopy [XPS], and Secondary Ion Mass Spectroscopy [SIMS] (Watts, J. and Wolstenholme, J. 2008). These techniques employ sputter depth profiling to determine in-depth atomic composition in thin films, although optimum depth resolution and a correction may be required to account for alternating materials and different sputter rates.

Considerations were made to reported results of previous characterization efforts on similar samples. Based on FTIR spectra Janicki et al. (2012) suggests that Niobium pentoxide and silica are well mixed at the atomic level and will not reflect significant mixture of phases. It must be noted that in reflectivity measurements, the effect of any interfusion at the interface is comparable to that yielded due to interface roughness (Gupta et al, 2003). The averaging aspect of the interface width concept is clear from the fact that a chemically intermixed in comparison to a physically rough interface result in identical profile functions. Furthermore, (Ghafoor, N. 2005) supports this notion and has observed that reactive sputtering of metals is more likely to promote an amorphous layer structure if the individual layer thicknesses are below some critical limit for crystallization and so long as this threshold limit is not exceeded the amorphous layers do not convert into polycrystalline layers.

2.6.1 Characterisation Theory and Governing Equations

The characterization methods employed in this project are based on certain fundamental principles which are key to interpretation and analysis of measurements conducted. This section of the literature survey aims to provide a brief introduction to these methods, defining key equations and nomenclature subsequently used.

2.6.1.1 Optical Reflectivity

Optical techniques determine film characteristics by measuring the interaction of the film with light and provide information on the thickness, roughness and optical constants of films. In conventional specular and diffused reflectance spectrophotometry, incident light reflects off the interface between layers in a multilayer stack and the air, the same effect is present at the interface between the film and the substrate (or the next intermediary layer), forming interference patterns by scanning the sample throughout a range of incident wavelengths.

2.6.1.2 X- Ray Diffraction

X-ray diffraction is based on Bragg's Law for constructive interference and it is a non-destructive which necessitates minimal sample preparation, X-Ray Diffraction signal is a result of an elastic scattering of monochromatic X-ray by core electrons of atoms in a sample. X-rays are diffracted due to the regularly-spaced atoms in a crystal lattice, producing the well-known XRD patterns, analogous to diffraction of visible light by gratings. Lattice parameters are the most important physical quantity in XRD as periodicity in atomic placement is the physical property that gives rise to XRD peaks (Whiteside, Chininis, and Hunt, 2016). It provides information in relation to film composition, texture, degree of crystallinity. The Bragg's Equation below formulates the underlying principle of this spectrophotometric method.

$$2d_{hkl} \text{ Sin } \Theta = n\lambda$$

Where d is the separation between parallel of atoms and represents geometric function of the size and shape of the unit cell planes otherwise known as Bragg's spacing, Θ is the Bragg angle and it is given by the angle of incidence of the X-ray , n is the diffraction order, and λ is the X-ray wavelength. The term Bragg planes refers to planes that are comprised of these constructively diffracting atoms.

2.6.1.3 X-Ray Photoelectron Spectroscopy

In X-Ray photoelectron Spectroscopy a soft X-ray (normally $Al_{K\alpha}$) basically displaces an electron from one of the energy levels in a material and all the X-ray energy is transferred to the electron. The use of a monochromatic X-Ray excitation source is encouraged since the photoelectrons kinetic energy is largely dependent on the excitation source. XPS is conventionally performed in an ultra-high vacuum environment to enable the photoelectrons the necessary mobility to reach the electron analyser without being scattered by gas molecules. The electron binding is a term used to refer to the energy required to remove an electron from its orbit to an infinitely remote point. It is characteristic of the energy level from which the photoelectron was emitted. The binding energy is given by the following equation obtained from (Baker, 2017):

$$E_B = h\nu - E_K - W$$

Where E_B = Binding energy, hν = X-ray energy, W = work function, E_K = photoelectron kinetic energy. XPS is commonly combined with ion sputtering to generate3 in -depth profiles

2.6.1.4 Atomic Force Microscopy

This method exhibits disparate principles from the techniques discussed hitherto which have been based one form of radiative reflection or the other, Atomic Force Microscopy technique operates on the principle of direct measurement of the deflection and the resultant oscillation of a flexible microscopic cantilever tip produced by attractive and repulsive atomic forces. In the tapping mode, the lever is driven by a sinusoidal wave and the curves are displayed as force versus time or force versus distance .The resulting frequency is then a characteristic of the surface being analysed.The oscillations generated are a result of atomic forces and AFM does not necessitate conductive samples as is the case with scanning electron microscopy and XPS. Consequently, AFM is capable of characterizing surface properties in addition to surface geometry because the tip effectively measures the strength of atomic forces (Whiteside, Chininis and Hunt. 2017). Different roughness parameters can be calculated as the standard deviation of all pixel values from the mean. However, RMS roughness (Rq) is conventionally used to describe the surface finish in the field of optics. Note, RMS roughness is the standard employed in characterization of optical surface profiles.

$$Rms = \frac{\sum_{\substack{x=1,N \\ y=1,M}} (Zxy - \overline{Z})\text{^}2}{(N-1)(M-1)}$$

Where N and M are the number of pixels in the x and y directions, $Z_{x,y}$ is the image pixel height with respect to the center plane height.

2.6.1.5 Scanning Electron Microscopy & Energy Dispersive X-Ray Spectroscopy

This electron beam method uses secondary produced electrons to computationally generate a two-dimensional image of the sample of interest ultra-high vacuum chamber. When incident on the sample,

the SEM electron beam loses energy through various mechanisms which cause the electron to undergo inelastic scattering and change of direction. The backscattered electrons are the high energy electrons which are elastically scattered and commonly poses the same energy as the incident electrons. The linear dependency of atomic number and backscattered allows for distinction of elements with wide atomic number gap

EDS involves the displacement of an electron from a core level in the atom. X-rays are emitted to release excess energy when an electron from a higher energy level drops into the inner core level. The equation below determines the energy difference between the higher and lower energy levels involved, this is facilitated by the fact that energy core levels involved in the process are specific to elements and as such are used to identify the elements present in the material.

$$EX_{RAY} = E_K - E_{L1}$$

Where $E_{X\text{-}RAY}$ = Energy of X-Ray, E_K = Energy of inner core level (k -level), E_{L1} = Energy from higher outer level (L1- level).

2.7 Conclusion

Thin film features such as surface roughness, interface roughness, degree of crystallinity and layer thickness are increasingly of growing interest in material science for various reasons. It is important to reiterate that high quality thin films can act as excellent optical reflectors which play vital roles in the modern solid-state laser systems. The day to day applications of dielectric multilayers include the temperature and optical sensors which can be found in high power projection systems. For optical films especially, it is often desirable to minimize the surface and interface roughness. The study of roughness is particularly important as it yields insight into morphology and topography of the surface which prove to be useful in synthesis and refinement of Physical or Chemical Vapour Deposition process parameters. In addition, the growth kinetics are better understood from roughness measurements of deposited films, as a result, it is expected that the findings in this project facilitate changes in process parameters at Plasma Quest Limited. The principle of an optical reflector is interconnected with the existence of the high-reflectance bands or photonic band gaps (PBG) in some certain frequency (or wavelength) ranges in Computers as a characterising the optical constants and performance of these films is imperative to understand their behaviour in application.

3 EXPERIMENTAL METHODS

3.1 Overview

The current investigation involved sampling and analysing three distinct multilayer samples deposited on silicon and glass substrate. The samples were deposited by Plasma Quest limited located in Hook, South West England. A total number of 6 samples were examined and analysed, the coatings were deposited on glass and silicon substrates. The samples were packaged and stored in carefully in plastic zip lock bags, each bag containing a consistent periodic multilayer stack deposited on glass and silicon substrate, that is 7 ,11 or 15 layers on either silicon or glass substrate. The package samples were transported to the Micro-Structural Studies Unit (MSSU), also called the electron microscopy facility of the University of Surrey where they were analysed using standard methods of characterisation. The nature of the measurement techniques employed and the necessity for a conductive sample in some cases denoted that the samples on silicon substrate were preferred for characterization. Prior to conducting some of the experimental procedures in this project a sample preparation was required. Due to the broad range of characterization

techniques expected to be employed to derive meaningful insight in this project, the author has collaborated with several Technical Staff and PHD students at the University of Surrey. Hence, in some cases the methods in this section are described as a concise summary of machine specifics and analysis procedures, rather than detailed steps involved in measurement.

3.2 Sample Preparation Procedures

The samples deposited on silicon were initially cleaved by etching with a diamond scribe and subjecting the samples to a subtle amount of pressure along the crystallographic planes. This is done to obtain desired sizes which fit on sample holders. Consequently, to provide a polished cross section which guarantees a satisfactory level of resolution in imaging and to facilitate desired conductivity of the multilayer samples in the vacuum chamber. The sample preparation procedures carried out involved setting the samples in a mixture of Epoxy hardener and Tepofix resin, the respective volumes of hardener and resin present in the mixture consisted of 1:7.5 ml poured into hot water. With the samples clipped into a 30 ml mould the mixture was added in and allowed to set for a designated period. After letting the mixture settle for 8 hours, the resultant solid mould was polished using the ATA SAPHIR 520 to achieve a fine texture which would aid visibility of the interface morphology and microstructure in the microscope. The machine specifics are as follows; Speed = 150 Rpm, Force = 10 N. The diamond suspension selected was 3µm and the lubricant utilized was alcohol based, this is the standard recommended for fine grinding and polishing of most materials. The abrasive employed was a silicon carbide sand paper. A systematic step by step procedure involving polishing for 45 seconds, followed by rinsing with warm water for 10 seconds and then rinsing with isopropanol for another 5 seconds was adopted. The sample was dried with an air dryer to blow off any possible surface asperity.

Consequently, the samples were also gold coated on the EMITECH K575X instrument with a 2nm coating using argon as the working gas in the sputter depositor. Gold coating was chosen due to its low work function which makes it susceptible to perform efficiently as a thin conductive coating. Also, minimal heating of the sample is incurred in the process due to the cool sputter nature of gold. Additionally, it is noteworthy to indicate that gold coating permits imaging of non-conductive samples at higher voltages, this corresponds to a smaller effective beam diameter and higher resolution on the SEM. Consequently, were high magnification imaging with low atomic number samples is desired gold coating is considered advantageous. After gold conducting, the samples are laced with copper tape to provide a path way for the electrons from the sample holder to the sample mould. A detailed account of each preparatory

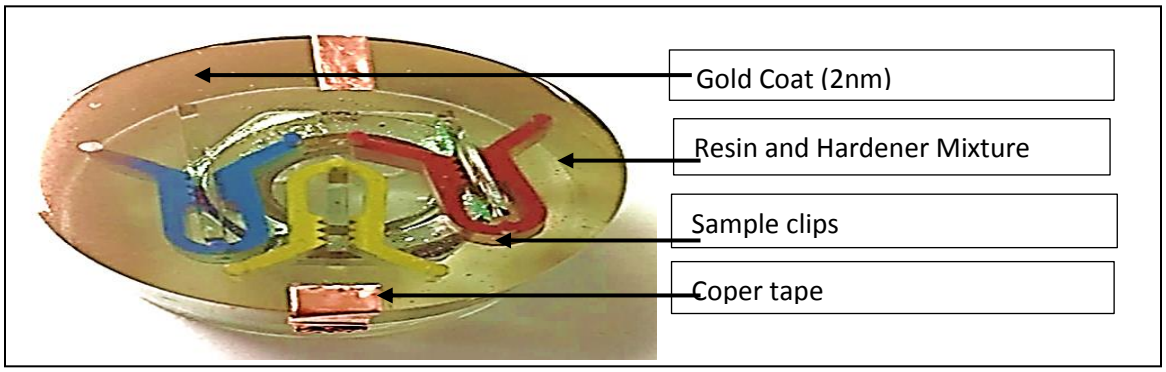

Figure 5: Finished metallurgical polish of sample preparation for Multilayer samples deposited on glass substrate. 7, 11 & 15 layer mounted in blue yellow and red peaks respectively.

operation undertaken to attain the sample readiness state as shown in figure 5 is given to facilitate traceability and repeatability of this project work.

3.2.1 Adhesive Tape Test

A shear peel of test was performed on the 11 and 15 multilayer samples deposited on glass substrate to observe the adhesive quality of the surface of the multilayer to the underlying interface. The test is able to distinguish based on a self-assigned scale distinguishing between complete lifting, partial lifting or complete adhesion. The peel off test was performed by sticking Scotch Tape on the surface, consequently the tape is ripped off at a uniform rate and an angle of 60˚. The test performed is the simplest means of assessing the adhesive performance of the film and it can be made semi qualitative by controlling the angle of pull and the rate of pull.

3.3 SEM and EDS Equipment and Analysis Parameters

A JEOL JSM-7100 Field emission - Scanning Electron Microscope (FE-SEM) with a hot (Schottky) electron gun was utilized for verification of the multilayer thicknesses by providing information about the sample surface and cross section. It is an ideal technique commonly employed for imaging and analysis of micro- and Nano-structures, the instrument is fitted with an EDS detector as illustrated in figure (6). The machine specifics during imaging are as follows; (accelerating voltage, probe current and working distance were 5 kV, 8 pA and 10 mm respectively).The vacuum chamber was operated at a working base pressure of 5.1 E-4Pa, the accelerating voltage and probe current was varied for imaging with the various detectors, the dead time recorded ranged between 20-22% for images taken for Energy Dispersive X-Ray Analysis (EDXA). Imaging was performed under the same conditions for the 7, 11 and 15 layer multilayers after sample preparation via gold coating or carbon coating. The Secondary electron detector and the backscattered scattered electron detector were used to facilitate the deeper analysis required during imaging. All three samples were examined under these conditions, the contrast and magnification employed were alternated and backscattered imaging was performed to distinguish the low and high atomic number elements in the sample. The application used for image editing and analysis is the Pathfinder Version 1.1 Microanalysis Software.

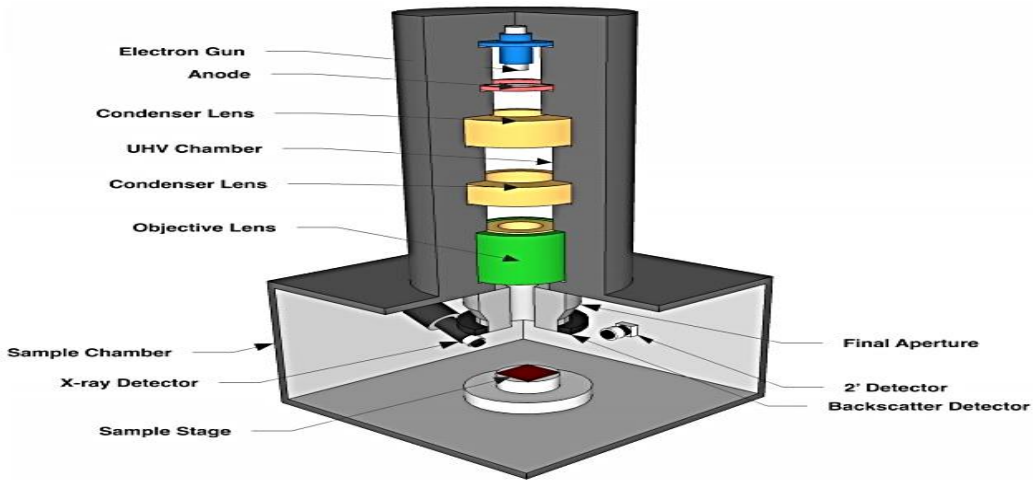

Figure 6: Scanning Electron Microscope schematic illustrating multiple detectors.

3.4 XPS Equipment and Analysis Parameters

X-ray photoelectron spectroscopy (XPS) is a surface analysis technique commonly utilized to determine elemental and chemical state information about a sample. XPS depth profile analyses were carefully conducted in this project using a Thermo-Fisher Scientific Instruments K-Alpha+ spectrometer manufactured in (East Grinstead, UK). The equipment is located in the Micro-Structural studies unit at University of Surrey. XPS depth profile analyses were performed on a ThermoFisher Scientific Instruments (East Grinstead, UK) K-Alpha$^+$ spectrometer equipped with Ar^+ Monatomic ion Beam and Ar_n^+ gas cluster ion beam (GCIB) sources. High resolution spectra were acquired using a monochromated Al Kα X-ray source ($h\nu$ = 1486.6 eV) operating at power of 300 W. An X-ray spot diameter of 200 µm radius was employed. Survey spectra were acquired employing a Pass Energy of 200 eV and the Ar ion gun was fixed at an angle of 45° to the sample surface. The raster beam High resolution, core level spectra were acquired with a Pass Energy of 50 eV and a step size of 0.1 eV. Semi- Quantitative surface chemical analyses were calculated from the high resolution, core level spectra following the removal of a non-linear (Shirley) background and used the Wagner sensitivity factors. The manufacturers Avantage software was used which incorporates the appropriate sensitivity factors and corrects for the electron energy analyser transmission function. All spectra were charge referenced against the C1s peak at 285 eV to correct for any charging effects during data acquisition. The depth profiles were acquired using the monochromated Al Kα X-ray source while sample etching was achieved using a ThermoFisher Scientific Instruments (East Grinstead, UK) MAGICS. The MAGCIS ion source permits depth profiling of soft materials using gas cluster ions as well as profiling layers of harder materials like metals or silicon using monatomic ion beam. As a result the clustered depth profile herein is incomplete as it would take a sufficiently long time to etch through all layers.

Ar^+ ion source was operated in the monatomic mode at 500 eV delivering 1.3 µA of Ar^+ etch current and in the GCIB mode at 8 KeV Ar_{150}^+ delivering 10 nA of etch current. The Ar^+ etch area was 1mm^2 to avoid the incidence of crater edge effect and the etch rate was determined using the layer thicknesses supplied by PQL and the etch times observed on the depth profile. The Advantage software was employed for peak fitting using a gauss/Lorentz mix ratio obtained by utiling a binding energy separation of 2.72 eV on the characteristic niobium doublet observed in the steady state region of the monatomic depth profile. Limiting parameters which cause ambiguity in the depth profile reconstruction were accounted for, an attempt to estimate the depth resolution function for the monatomic Ar^+ ion beam incidence was conducted using estimations for mixing length, information depth and surface roughness.

3.5 AFM Equipment and analysis parameters

A Bruker Dimension Edge AVH-1000 Atomic Force Microscope housed within an acoustic hood and mounted on a vibration isolation table was used to perform AFM analysis on the multilayer samples investigated in this project. Imaging was performed with the aid of ScanAsyst and was analysed using Nasoscope Analysis software. ScanAsyst employs Peak Force Tapping mechanism, which decouples the cantilever response from resonance dynamics and automatically adjusts all critical imaging parameters. This allowed automatic image optimization for faster, more consistent results, regardless of user skill level. Also, ScanAsyst optimizes the gain according to current sample condition at different locations and enables control of the image quality scans linked to complication of the tip surface interactions and

cantilever dynamics. This yields less artefacts in comparison to the conventional contact mode. Furthermore, in tapping mode the cantilever probe is excited to vibrate by an integrated piezo actuator. The amplitude of the forced oscillating lever is detected, analysed and utilized in the feedback loop. Closing the Z feedback loop in the AFM to minimize monitored oscillatory changes enables topography imaging. Each image displayed in the results section consists of 1024-line scan, the scan rate applied was 6.0 µm/s and the scan size was 10 µm. The stylus instrument used has a serial number 3B1931 and is made from silicon nitride (Si_3N_4), and a V-shaped cantilever with the following specifics; (Resonance frequency, f_0= 70 kHz and stiffness constant k= 0.4N/m). Engaging the device in tapping mode requires that the set point voltage to be smaller than the RMS voltage when the distance from the probe to the sample is large. The ScanAsyt algorithm optimized the set point such that the minimum force required to track the set sample surface controls the scan rate and automatically lowers the z limit if necessary. Nasoscope analysis software was employed for analysis, before surface roughness profiles for the samples investigated could be obtained, the unwanted features from the generated profiles [bows and tilts] present in the image generated were excluded by applying the flatten function. This a standard procedure on commercial AFM instruments to account for the fact that nearly all samples may be macroscopically tilted with respect to horizontal scan directions of the microscope. Multilayer samples and tips were protected from damage by direct force control at ultra-low forces performed by ScanAsyt. The AFM is calibrated and ScanAsyst takes care of the thermal tuning and laser alignment.

3.6 GIXRD equipment and analysis parameters

During this project, standard Grazing Incidence Angle Diffraction (GIXRD) has been performed. This is essentially an X-Ray powder diffraction measurement done with a fixed, very low incidence angle (1°- 3°). In other words, by fixing theta at shallow angles, X-rays are focused in the surface of the sample. The technique possesses enhanced surface sensitivity compared to standard (Θ -2Θ) and the measurement geometry is particularly useful for increasing signal based on the spot size due to the X-ray flux on the sample being more evenly spread over a wide area, especially regarding thin film samples. The measurements were performed on the Panalytical X'Pert Pro located in the Chemistry laboratory (AZ03) at the University of Surrey. The multilayer samples utilized were deposited on glass and silicon substrates. The experiments were conducted with the following instrument specifics: {Cu K-alpha generated X-ray radiation with ʎ = 1.5406 nm; generator set to 45kV/40mA; X-ray mirror used to focus the beam; diffracted beam measured using a Geiger-Muller type detector (Monochromatic graphite detector), incident beam placed at a low incident angle. The physical quantities which give rise to the XRD peaks are the crystal planes and a methodical approach has been adopted to identify and verify against standard databases. It is important to note that glancing angle measurement was carefully selected out of the range of XRD methods available, the rationale behind this being the spot widening effect which occurs. This effect reduces X-ray flux on the sample and decreases X-ray damage and should potentially be less likely to penetrate through the multilayer samples as shown is figure 7, this results in higher signal and reduced background (Widjonarko, N. 2016). However, the experiment conducted reflected signs of instrumental error and will be discussed extensively in the result analysis and discussion section.

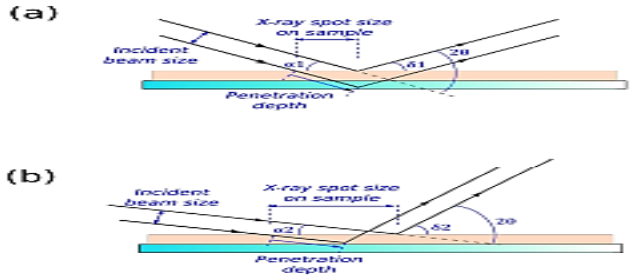

Figure 7: Illustration of spot size widening in GIXRD (Widjonarko, N. 2016).

3.7 Optical Reflectivity

Specular and diffused reflection were performed on the Cary 5000 to measure the transmittance of the multilayer films, the machine is essentially a dual beam spectrophotometer consisting of a light source, iterating sphere, sample holder and two detectors. It is able to make transmission or absorbance measurements between 175 nm and 3300 nm. It can measure optical properties in the Ultraviolet-Visible-Near Infrared Rang. A zero-baseline correction factor was applied to compensate for sample holder in the apparatus. The spectral contributions of the samples was accounted for by calibrating the spectrophotometer for background noise with a polytetrafluorethylene (PTFE) glass slide. Although, PTFE has high reflection qualities with a reflection coefficient of up to 98 % in the broad wavelength range of 250 to 2,500 nm it has not correctly applied the 0% baseline correction for the sample holder appropriately, this has resulted in an observed effect of noise in the spectrometer. It is important to note that the sample must be large enough to cover the beam image (i.e. the hole). The sample size requirements has not been properly accounted for in sample preparation and as a result the 7 layer sample was not cleaved to the appropriate size to fit the sample holder. Therefore, there is no data set included for this particular multilayer sample in the results section. An illustration of the schematic employed is shown in figure 8.

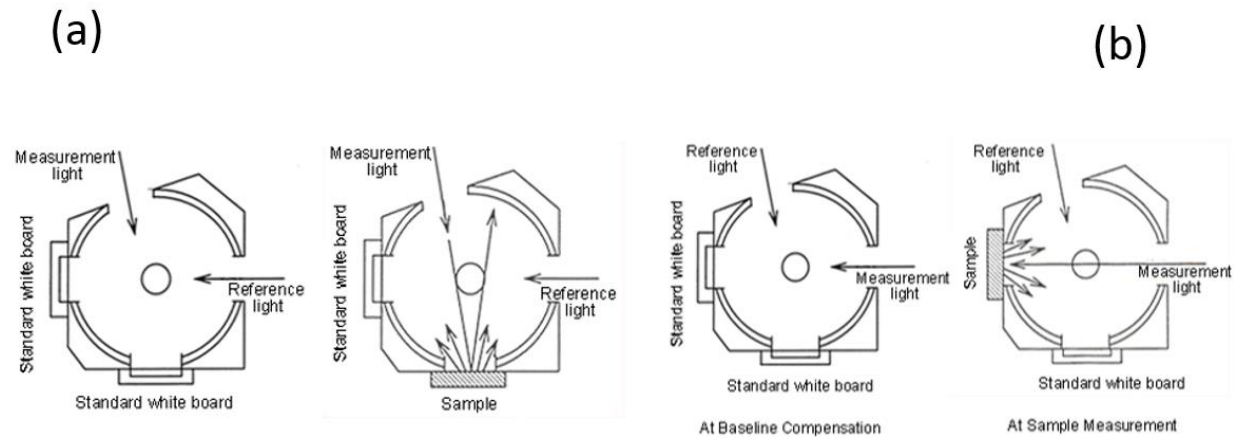

Figure 8: (a) Apparatus for Measurement of diffused and specular reflectance (b) Measurement of diffused reflection only. Instruments, S. (2018)

4 RESULTS & DISCUSSION

4.1 Compositional Study

XPS survey spectra of the dielectric multilayer films is shown in figure 9, measurement of the chemical profiles of O1s, Si2p, and Nb3d peaks were carried out on the surface prior to sputtering and after sputtering for different time periods as the XPS technique is most sensitive to the outer surface atomic layers, therefore the spectra have been collected from the steady state region of the 1st Nb_2O_5 layer and on the [Nb-Si] and [Si-Nb] interface regions, the following spectra are shown in figures 10-12 . The interface was defined as the midpoint between the silicon and the niobium steady state peak positions in the depth profiles. Since only photoelectrons which have not lost energy (through inelastic scattering) prior to escaping from the surface contribute to the peaks observed in the acquired XPS spectra, the photoelectrons that have lost energy contribute to the background and are not shown on the survey in

figure 9. The different Niobium oxidation states are emphasised upon in the analysis because it is more susceptible to preferential sputtering of oxygen and Niobium enrichment in comparison to the SiO_2 layer and is consistent with findings by Hoffman and Sanz as shown in the appendix. This is consistent with the depth profiles in shown in figure (1a). The various oxidation states of the mixed Nb oxide phase were thus further investigated by peak fitting the Nb 3d peaks on the first (surface) Niobium oxide peak.

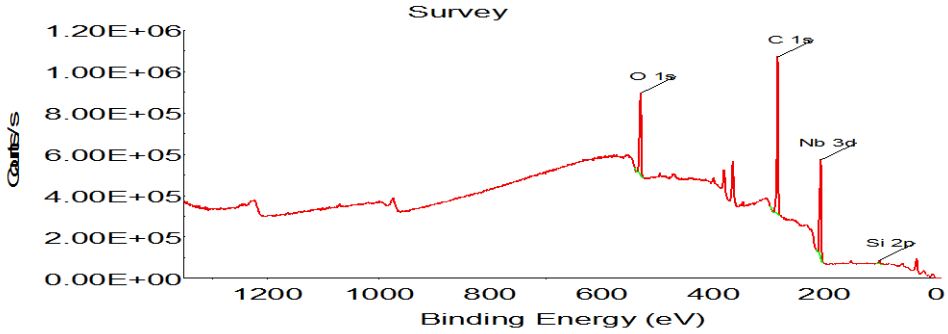

Figure 9: XPS Spectra acquisition survey

In figures 10 - 12, it should be noted that (a), (b), (c) denote Nb3d, O1s and Si2p snaps respectively. Using etch time and level one can deduce a better visualization of thre transition through the surface.

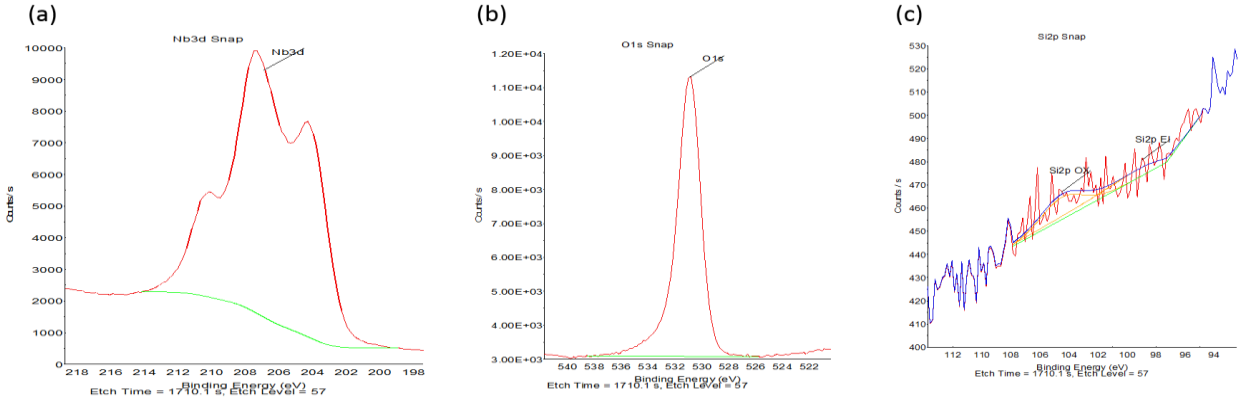

Figure 10: Snapshot taken at niobium steady state peak (Etch time = 1710.1 seconds, etch level = 57)

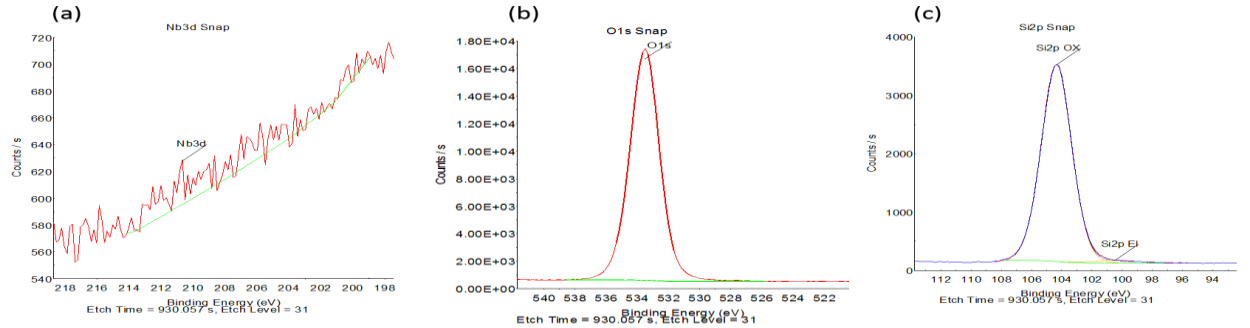

Figure 11: Snapshot taken at silicon steady state level. (Etch time = 930.05, Etch level = 31)

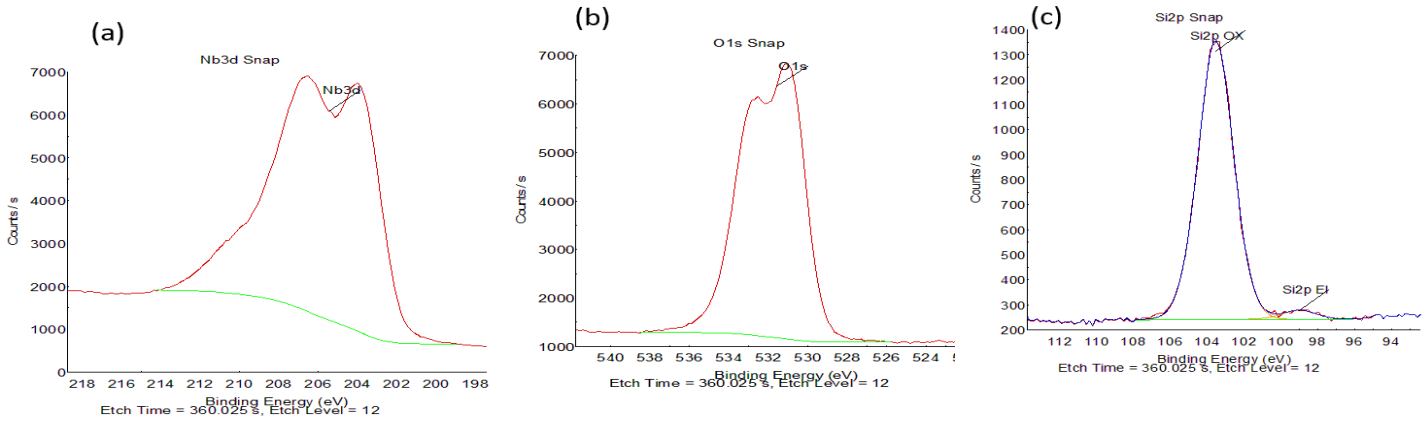

Figure 12: Snapshots taken at Niobium oxide -Silicon Interface transition region. (Etch time = 360.25, Etch level = 12)

4.1.1 XPS Spectra and Depth Profiles

Quantification of the measured sputtering profile was accomplished by appropriate methods of profile reconstruction. First order non-linear effects like preferential sputtering were corrected by a composition dependent relation between sputtering time and depth. Also, the non-linear relationship between intensity atomic concentrations was corrected by applying a composition dependent sensitivity factor. The compositional purity of the deposited films is indicated by the fact that no peaks are observed other than Nb3d, O1s, Si2p and adventitious Carbon (C1 s). It should be noted that the carbon contamination layer was not of interest in this project and as a result have been excluded from subsequent depth profiles. From the core level spectra of Nb3d electron orbital, the characteristic doublet peak is observed at binding energies of 207.3 eV and 210.4eV which corresponds to Nb $3d_{5/2}$ and Nb $3d_{3/2}$ respectively and is in agree met with literature data. To further investigate the notion of the probable five-valent niobium (Nb^{5+}) sub oxide states which may be identified in the deposited multilayer films after sputter etching, a peak fit has to be performed. Consequently, the core level peak of oxygen (O 1s) was found to possess a binding energy of 531ev as measured on the niobium steady peak region, a slight chemical shift is observed in the silicon steady state region where the O1s binding energy was estimated as 534 eV. The O1s Spectra at the interface indicated by a doublet signifying a change in chemical state induced by the percentage contributions of oxygen from NbO and Nb_2O_5 sub-oxides, it is found that NbO contributes 17.85% and the corresponding contributions from Nb_2O_5 based on stoichiometry is 45 %. These percentages were obtained from the Nb 3d spectra fitting procedure, cumulatively NbO and Nb_2O_5 contribute 63.7% and this shows good agreement with the depth profile in figure (10a)

The steady state composition for the oxides in the multilayer stack at incident energies of 500 eV and 3 Kev have been estimated and are shown in table 2 below. The steady state composition of niobium pentoxide at 500 eV and 3KeV is ($NbO_{1.57}$) and ($NbO_{1.05}$) respectively it shows a good agreement with findings in (Baker et al., 2017) who found the steady state of tantalum pentoxide under 500 eV and 3KeV Ar^+ ion bombardment to be ($TaO_{1.50}$) and ($TaO_{1.55}$) respectively.

Table 2: Steady state atomic percentage composition of multilayer films based on bulk oxide and XPS calculated Stoichiometry.

Deposited Oxide	SiO_2		Nb_2O_5	
Stoichiometry	At (%) of Oxygen	At (%) of Si	At (%)of Oxygen	At (%) of Niobium
Original	66.6	33.3	71	29
Monoatomic profile	65	35	61	39
Clustered profile	66	34	65	35

Table 3: Quantification of the degree of preferential sputtering observed in the multilayer stack. All ratios obtained are calculated relative original bulk stoichiometry as stated above.

Ratio of elements	Original	Monoatomic *(500 eV Ar+)*	Clustered *(3keV Ar_{150}^{+})*	Experimental result	Literature data (J.B. Malherbe et al.,)
(Nb/O)	0.4	0.64	0.53	1.57	2.22
(Si/O)	0.5	0.54	0.52	1.05	1.00

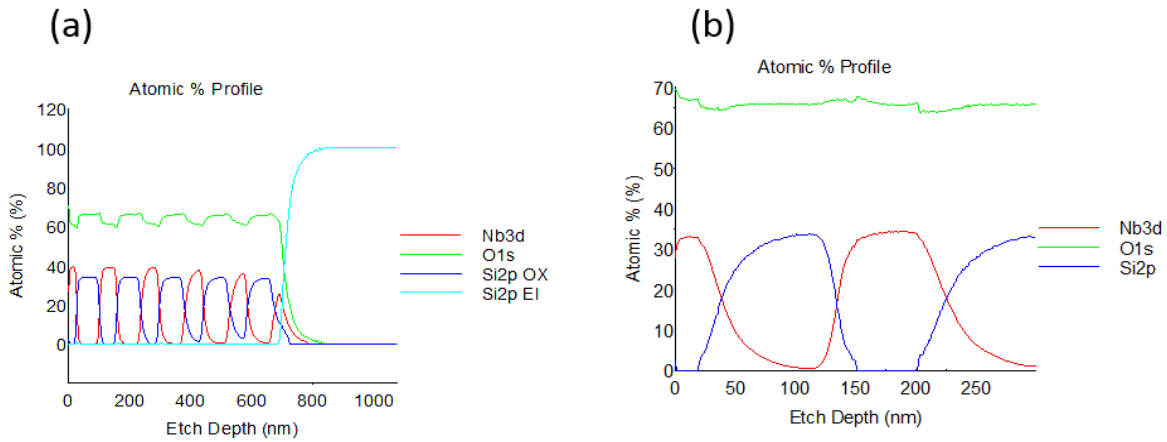

Figure 13: **(13a)** *XPS depth profile of 11 layers of Nb/Si obtained with 500 ev Ar+ ions at 45° incidence. The first Nb layer is estimated to be 23.98 nm before the onset of mixing. Sputtering rate ratio r (Si/Nb) = 1.003.* **(13b)** *3kev Ar_{150}^{+} profile, measured depth of corresponding first layer is 25nm, ratio r (Si/Nb ratio r (Si/Nb) = 0.91.*

A series of over checks were performed to validate that the stoichiometry of Nb_2O_5 calculated from the XPS data in relation to the actual bulk oxide stoichiometry are presented as a ratio of (Nb:O) and (Si:O). This is done to verify whether the right stoichiometry was attained across the 7, 11 and 15 layer samples. However, the composition of the multilayer films was determined by sputter etching in XPS prior to measurement, induced reactions resulting from the effect of preferential sputtering of oxygen under ion bombardment essentially causes lighter elements to be sputtered faster than heavier ones in the film

stack. This results in an observed enrichment of Nb_2O_5 due to the accumulation observed on the surface within the 5nm depth analysis for the XPS. Calculations performed to verify the degree of preferential sputtering observed yielded that the Niobium stoichiometry is increased by 34% in the monatomic depth profile in comparison to an observed 20.6% increase in the clustered depth profile as compared to the bulk oxide. The SiO_2 layer on the other hand shows only a 3% and 7.6% increase in silicon composition in the 500 eV Ar^+ and 3keV Ar_{150}^+ incident energy cases , this result is in agreement with the linear cascade theory of sputtering which stipulates that the amount of oxygen depletion increases with cation mass.

The etch rate for the two oxides present in the multilayer were determined from the monoatomic depth profile attained with monatomic ion bombardment Ar^+ (500 eV), the values were 0.077 nm/s and 0.075 nm/s for SiO_2 and Nb_2O_5 respectively. The ratio of the sputter rates calculate from the monatomic depth profile for Nb_2O_5 relative to SiO_2 yields 1.003, this value strongly correlates with findings by Baer et al. (2010) for values of 11 metal oxides with similarly calculated relative sputter ratios ranging between (0.8 – 1.2). Consequently for the 3kev Ar_{150}^+ clustered profile, there is less preferential sputtering of oxygen observed in comparison to the monatomic profile and ratio of sputter yields is 0.91, this result also follows the trend observed by Baker et al., (2017). The time intensive nature of clustered ion bombardment made it difficult to sputter etch through all 11 layers. As a result, the etch rate calculated from the incomplete clustered profile is less accurate, and a resultant error will be present in the etch time to depth quantification performed.

4.1.2 Peak Fitting

In order to establish the Nb chemical states detected during depth profiling of the Nb_2O_5 layer, a methodical approach was implemented in fitting the Nb3d spectra. Firstly, known values of the binding energies for the metallic niobium doublet and well reported peak positions of the Nb_2O_5 doublet were identified from literature. The initial Nb^{5+} peaks were fitted carefully to ensure the subsequent sub-oxide peaks which are generated due to preferential sputtering of oxygen from Nb_2O_5. Consequently, in fitting the Nb^{5+} peak envelope, the FWHM, L/G Mix ratio, the relative intensities and the separation ratios between $Nb3d_{5/2}$ and $Nb3d_{3/2}$ as obtained from , the rationale behind emphasis of this spectra is that in practise they are easily isolated and accurately fitted using the known binding energies of the metallic niobium doublet. Care was taken to ensure that these peaks appear at the correct binding energies as there is a relative positional influence of peaks on one another in the spectra. Residuals are a measure of the difference between the experimental data and the fitted data were also considered, the spectra indicated that the residual signal was multiplied by a factor of 5, indicating that the perfect curves are fitted to the experimental data within a reasonable level of accuracy. The Nb_2O_5 profile quantification of the possible sub-oxide reaction states that could have been generated during iron etching are Nb^{5+}, Nb^{4+} , Nb^{2+}, Nb^0 representing Nb_2O_5, NbO_2, NbO and Nb respectively. However only two oxidation states have been observed in the peak fitted below. The fitting parameters (binding energy and FWHM) are compiled in table 4 together with data from the literature survey. From this data, the percentage of oxygen contributed by both oxidation states is 20% and 42.8% for NbO and Nb_2O_5 respectively, this results in a total oxygen concentration of 62.8 %. This is in strong agreement with oxygen (01 s) atomic concentration of 61% obtained from the monoatomic depth profile in figure (10 a).

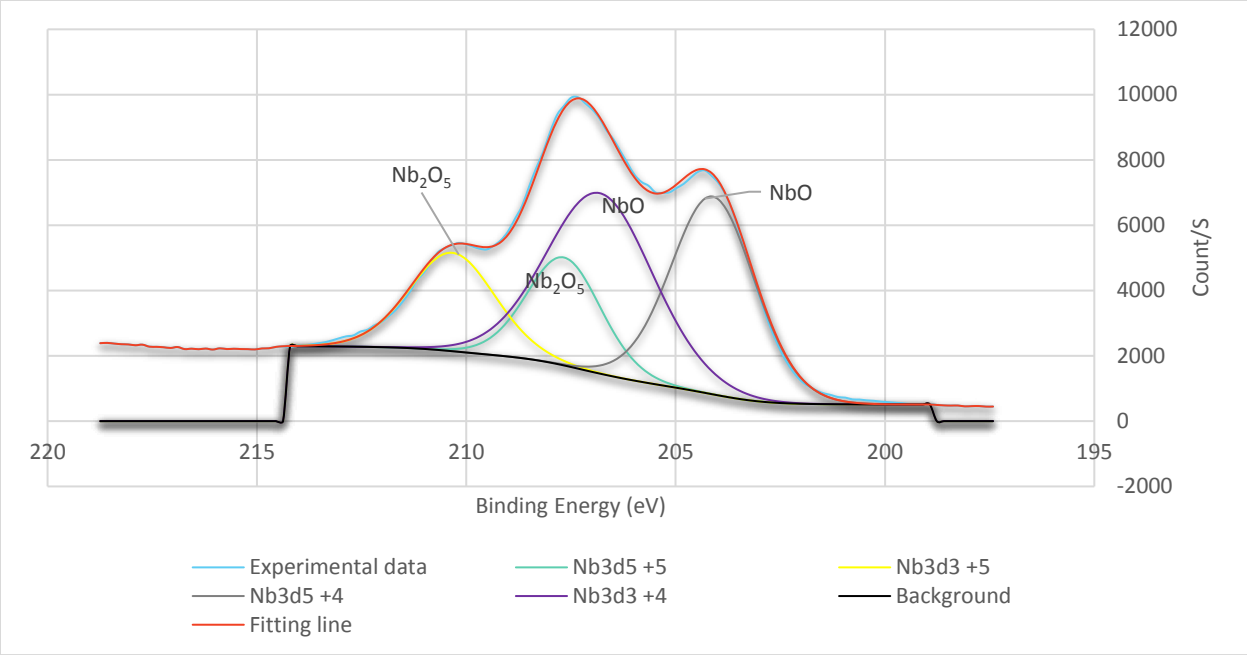

Figure 104: Peak Fitting performed on NB3d spectra indicating the peaks for different oxidation states

Table 4: XPS Nb 3d binding energies and FWHM in the peak fits for the niobium pentoxide depth profiles.

Sub oxide State	Line	Binding energy (eV)	FWHM (eV)	Literature Data- (Hoffman and Sanz) (eV)	Literature data- (Briggs & Seah 1988) (eV)
Nb_2O_5 (Nb^{5+})	Nb3d 3/2	207.4	3.23	207.4 ±0.2	207.6 ±0.2
(Nb^{5+})	Nb3d 5/2	210.4	2.43	210.2± 0.2	
NbO (Nb^{4+})	Nb3d 3/2	203.8	2.34	204.5±0.2	203.7 ±0.2
(Nb^{4+})	Nb3d 5/2	207.3	2.07	207.3±0.2	`

From table 4 we are able to deduce the presence of the (Nb^{5+}) and the (Nb^{4+}) oxidation states which were identified via peak fitting. The binding energies and FWHM values have been presented and verified against two independent sources. There is a strong agreement between the peak fitting performed in this experiment in comparison to literature, it is a bit odd that only two oxidation states have been observed and this may be indicative of the level of stoichiometry depletion which occurred during sputter etching. In research conducted by Hoffman and Sanz on 30 nm thick Nb_2O_5 there was an observation of for oxidations in comparison to 2 in this experiment. In essence, although the results in this experiment show good agreement with referenced data, there is an indication that they may be inconclusive and need to be subject to further analysis to confirm the presence of only two oxidation states.

4.1.3 Stoichiometric Study of Monatomic Depth Profiles

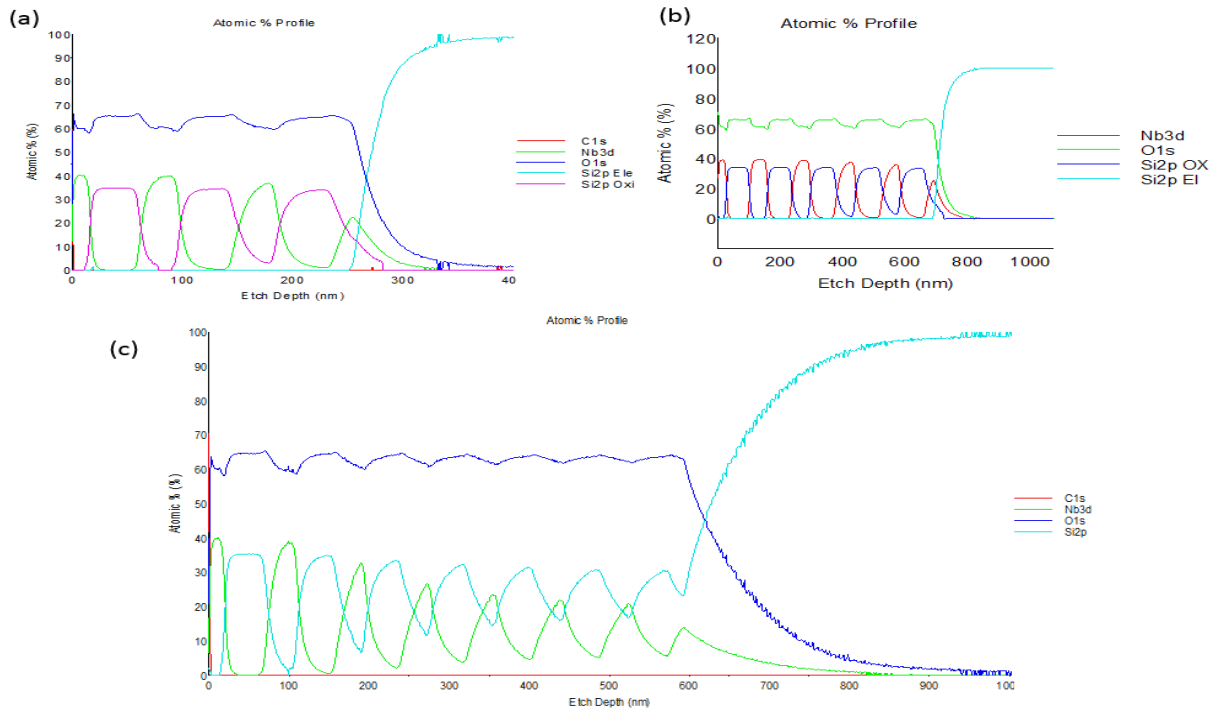

Figure 15; (a) 7 layer Ar^+ depth profile, (b) 11 layer Ar^+ depth profile (c) 15 layer Ar^+ depth profile

The stoichiometry of the 7, 11 and 15 multilayer films investigated and the depth profiles have been studied and presented in figure (15) , which confirms that the HiTUS deposited multilayer films are stoichiometric and the chemical compositions of the oxides present are consistent regardless of the number of layers in the stack, the results from the depth profiles indicate similar levels of preferential sputtering because the ion gun incidence angle and intensity were consistent across the monatomic % 500 eV Ar^+ sputter etched depth profiles for the 7, 11 and 15 layer samples. The premise of consistent stoichiometry implication agrees with absorption and transmission observed in the optical characterization.

4.1.4 Depth Resolution Function

Depth resolution is the term which refers to the depth range over which a signal increases or decreases by a specified amount between two media. By convention the depth resolution corresponds to the distance over which a 16-84% change in the oxygen signal is measured (Watts, J. and Wolstenholme, J. 2008). Depth resolution is commonly simplified as a useful description of the average composition in a depth range within which nothing is known about the shape. According to Watts and Wolstenholme (2008), the depth from which the electron is collected will affect the depth resolution. This follows the convention that the lower the kinetic energy of collected beams, the smaller the information depth which corresponds to a higher depth resolution. The depth resolution, was calculated from the depth profiles as the etch depth comparable to the region in which the oxygen (O1 s) signal drops from 84 -16 % of the maximum point at steady state region of the profile. The depth resolution on the monatomic

Ar^+ profile was estimated using the Mixing-Roughness-Interface model and over checked using the Avantage software analysis tools. The interface width was calculated as 5.22 nm and 5.76 nm for mixing length estimates of 0.4nm and 4nm respectively. Attempts to verify these results with the software yielded 5.95nm and 6.45nm which indicates a 14% scatter between both methods. Estimations for the mixing length are based on a range defined by (Baker, 2017).

4.1.5 X-Ray Diffraction Analysis

The HiTUS sputtered Nb_2O_5/SiO_2 multilayer films on glass substrates were examined by X-Ray diffraction to analyse their structural behaviour. The X-Ray diffraction results infer that all the multilayer samples (7, 11, and 15) are amorphous in nature. The XRD spectra for the 7, 11 and 15 layer samples are shown in figure 16 as a function of absolute intensity and 2 Θ. A survey was conducted for crystallinity, however, what we have found is an amorphous hump appearing between (30 - 47 Θ) on the 7 layer sample which corresponds to an amorphous halo on the 11 and 15 layer samples in the same region. Consequently the lack of clearly defined sharp peaks as would be expected from a single crystal or polycrystalline structure is supportive of the notion that dielectric metal oxides are amorphous in nature, this could be explained by the fact that crystal lattice orientations are not initiated due to low activation energy of sputtered atoms in the vacuum chamber during deposition. This constraint on the mobility of impinged atoms on the substrate surface is a potential underlying cause of the amorphous nature of the deposited films. (Coşkun and Demirela, 2013) have reported similar findings in their RF magnetron sputter deposited Nb_2O_5. Considering, the XRD spectra of the 15 layer sample, there is a progressive increase in the crystalline looking peaks with a decrease in the number of layers. However, it is expected that the samples examined would exhibit a lack of periodicity and a lack of the tendency to order in the sense that atoms are fairly tightly packed together and reflect a statistical tendency to display a particular interatomic distance. Consequently, the sharpness of the peaks is indicative of the presence of single silicon crystal substrates and in previous work using GIXRD, similar effects are observed which at the moment are unexplained.

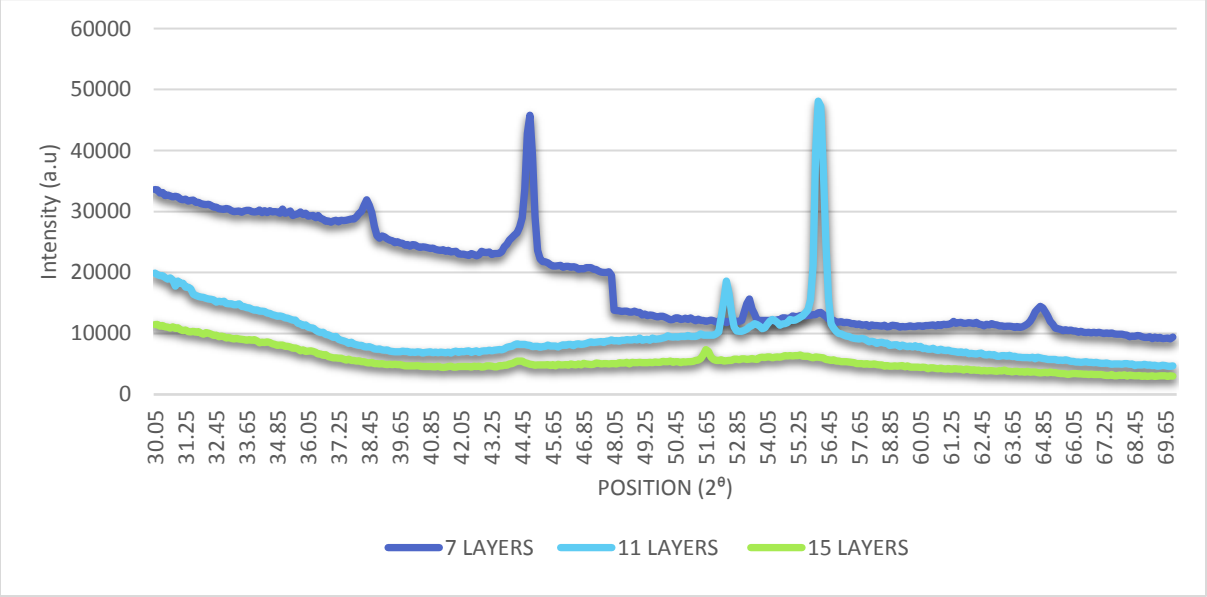

Figure 16: XRD Spectra showing 7, 11 and 15 layer samples.

The progressive shifts in the XRD spectra and the spurious peaks on the spectra may be attributed to the strain caused by changes in chemical composition, Cullity, B. (2015). These effects are reported to result in either poor particle statistics which cause random error in observed diffraction peak intensities or preferred orientation commonly observed in thin films which creates a systematic error in observed diffraction patterns. It is important to note that the multilayer samples examined in this project exhibit the properties of a glass- ceramic microstructure, in other words the diffraction pattern is not similar to single crystals and powder diffraction and the grains are not likely to be crystalline and randomly oriented. (Viana et al., 2006) have observed similar findings in work performed on anatase nanocrystalline TiO_2 films produced by a sol-gel process and also by Halindintwali et al. (2010) in their work on silicon-based films deposited using the hot-wire chemical vapour deposition (HWCVD) technique.

4.2 Surface Morphology and Topography

Scanning electron micrographs were taken to examine the morphology of the surface of the multilayer samples. The surface images reflected that the SiO_2 and Nb_2O5 films were fairly uniform and level and relatively smooth as shown in figure 17. XPS measurements confirmed that the impurities observed on the surfaces of the multilayer samples were mostly adventitious carbon and what is observable on SEM images below may be indicative of dust particles on the sample. The images shown as a comparison of the three samples investigated are low magnification images taken at (x500). Images taken at high magnifications on the SEM indicated no observable indication of a columnar structure indicating crystallinity but rather there is an observed intensification of the uniformity of the observed grey texture of the sample surface. This grey background increased with magnification up to 100,000, to see if we could identify presence of any columnar structure or periodicity on the surface which is characteristic of PVD manufactured films. Figure 15 has been included in the report as the only image taken at high magnification to illustrate the aformentioned point.

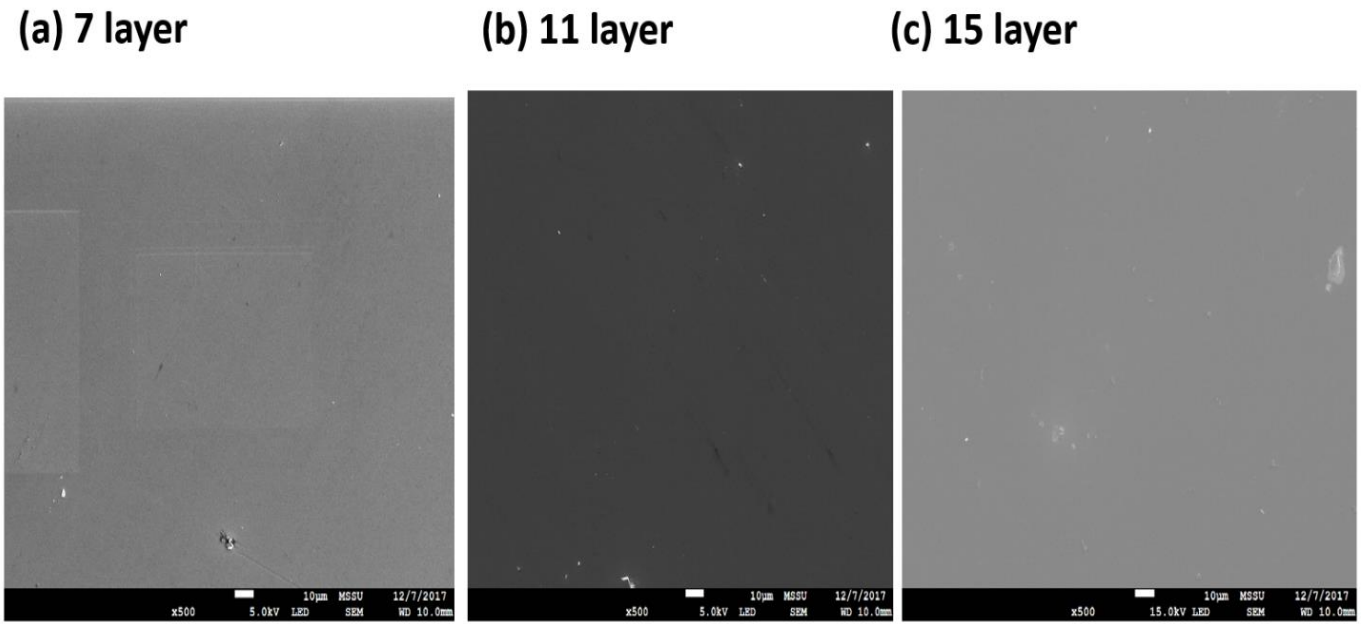

Figure 17: SEM surface images for the 7, 11 and 15 layer samples.

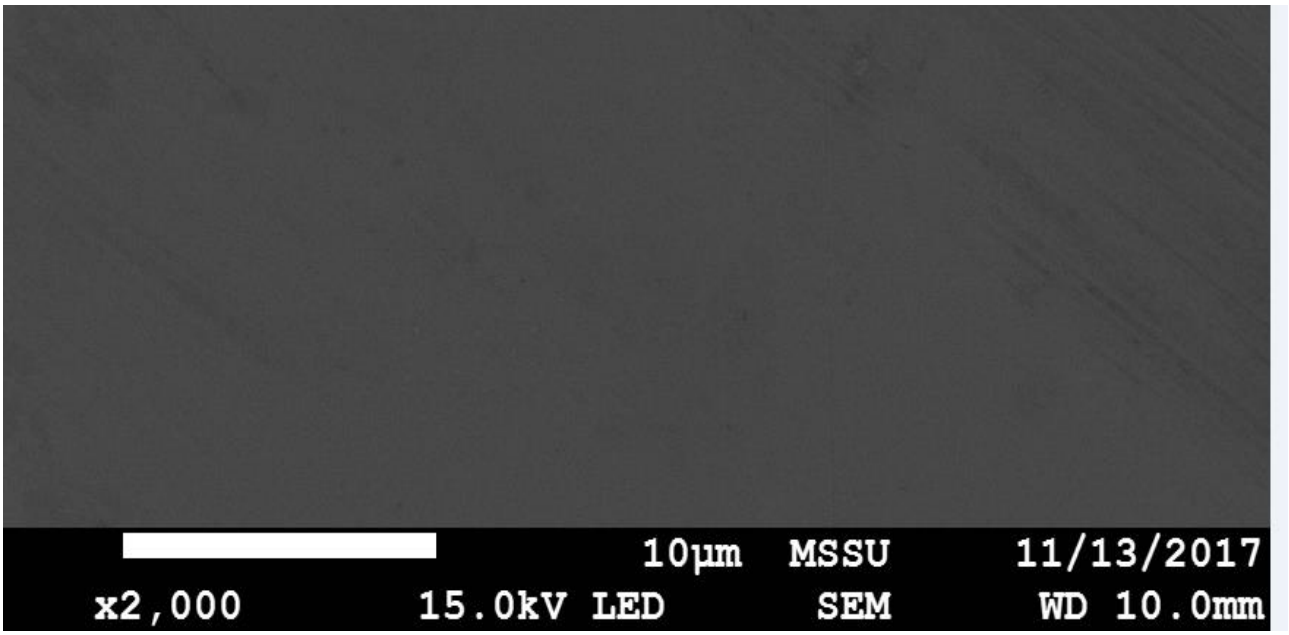

Figure 18: High magnification imaging of the surface for comparison against low magnification images

4.2.1 Preliminary EDXA Morphology Analysis

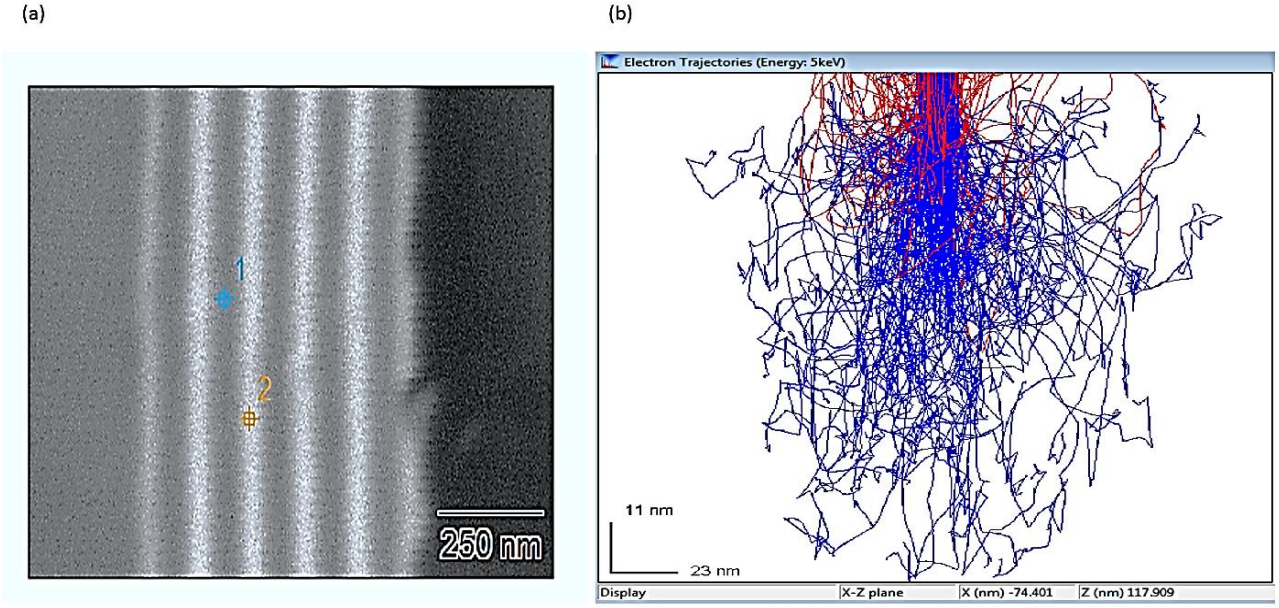

Figure 19: (a) EDXA point identification and (b) Calculated interaction volume for silicon dioxide and niobium pentoxide.

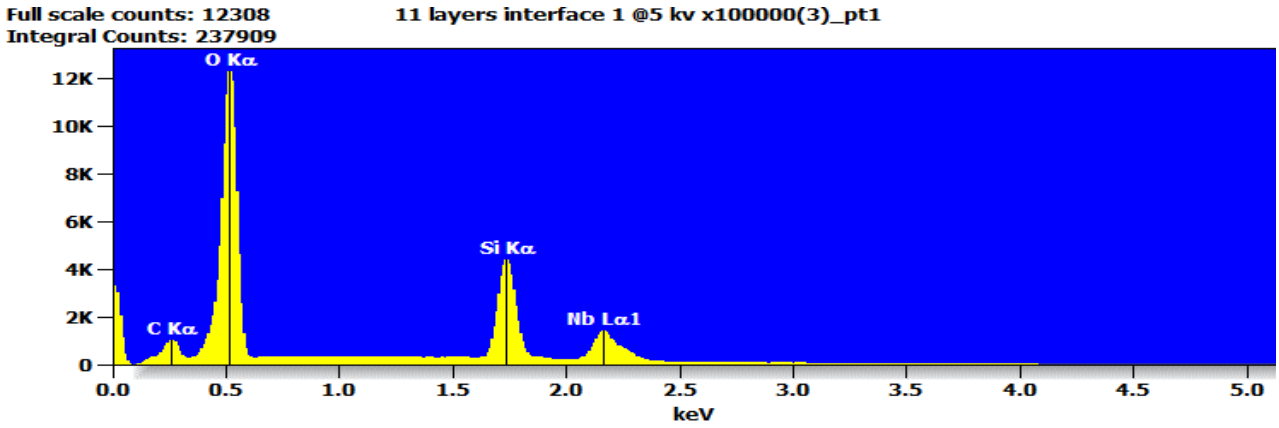

Figure 20: EDXA spectra of SEM cross sectional image shown in figure 16.

A preliminary study of elements in the multilayer was carried out via chemical characterization of the samples, this was carried out by EDXA analysis on the SEM cross section images collected. Point identification as shown in the image above was conducted on the points of interest. Point 1 corresponds to a SiO_2 layer and point 2 corresponds to the position of Nb_2O_5 layer within the multilayer stack. The interaction volume of the EDXA as calculated for SiO_2 and Nb_2O_5 is 117.9 nm as shown in figure 16(b) and this shows 5.98 % scatter with the manufacturers' data for the bilayer thickness which is 124nm at the middle of the stack. The observed spectra shown in figure 20 corresponds to the atomic percentages presented in table 5 for the aforementioned estimated interaction volume. Accurate material analysis via EDS necessitates the use of standard samples and material correction factors. Table 6 on the other hand gives an indication of the accuracy of the results obtained.

Table 5: Atomic Percentages of Elements within interaction volume

	C-K	O-K	Si-K	Nb-L
Silicon dioxide layer	2.4	61.9	24.7	10.9
Niobium pentoxide layer	3.9	61.5	18.2	16.3

Table 6: Atomic % Error (+/- 1 Sigma) based on atomic percentages tabulated above.

		C-K	O-K	Si-K	Nb-L
Silicon dioxide layer		±0.1	±0.4	±0.2	±0.2
Niobium pentoxide layer		±0.1	±0.4	±0.2	±0.2

4.2.2 Cross Sectional SEM Study

SEM cross-sectional micrographs show that periodic multilayer stack is relatively uniform and layer thicknesses measurements have been verified against the manufactured data to determine the accuracy

of the deposition process used. Although SEM has provided mostly qualitative data, it is expected that the data supplied by AFM would provide quantitative data which correspond to what is observed in the SEM surface images. THE SEM cross section images show good agreement in terms of total layer thickness, bilayer thickness and individual layer thickness when compared against the manufacturers thicknesses which have been obtained based on deposition time.

The data presented in table 7 is representative of the periodic 7 layer sample, indicating the quarter wave stack design having high index next to the substrate. The 7 layer sample has been selected as the case study for this section of the analysis because an anomaly has been observed on the cross sectional image. To deduce the source of this observed buckling of the structure, several probable causes have been explored. Since the regular progression of thickness throughout the stack is required to maintain the desired ranges or to extend the high reflection zone in dielectric multilayers. Essentially, this ensures that a sufficient number of layers in the stack have optical performance up to or near a quarter wave to yield high reflectance.

Table 7; Manufacturers deposition layer thicknesses verified by SEM imaging.

Layer position	Multilayer design (n)	Manufacturers thickness (nm)	SEM Measurements	Percentage error (%)
1st layer	H	24	25.3	5.13
2nd layer	L	76.5	77.8	1.6
3rd layer	H	48	48.8	1.6
4th layer	L	76.5	77.8	1.6
5th layer	H	48	48.8	1.6
6th layer	L	76.5	78.8	1.6
7th layer	H	24	25.3	5.3

The thickness obtained from SEM imaging are only qualitative, however they agree with reports in literature with regards to multilayer thicknesses obtained via optical characterisation. Janicki et al., (2012) reported that thicknesses obtained via optical characterisation were higher than those calculated from deposition rates. This effect has been explained by Janicki et al., as resulting from higher porosity outside deposition conditions, consequently it may also be due to inaccuracies in the measurement technique employed.

The thicknesses supplied by the manufacturer were subsequently employed to establish a correlation between the surface roughness and the interface width. Using the power law correlation between interface width and bilayer thickness. The power law correlation assumes the growth time restarts at each interface and is explored in more detailed in a subsequent section. The substrate information was also required when considering the concept of restarting growth as such figure 21 has been supplied by the manufacturer to facilitate this aspect of the multilayer investigations.

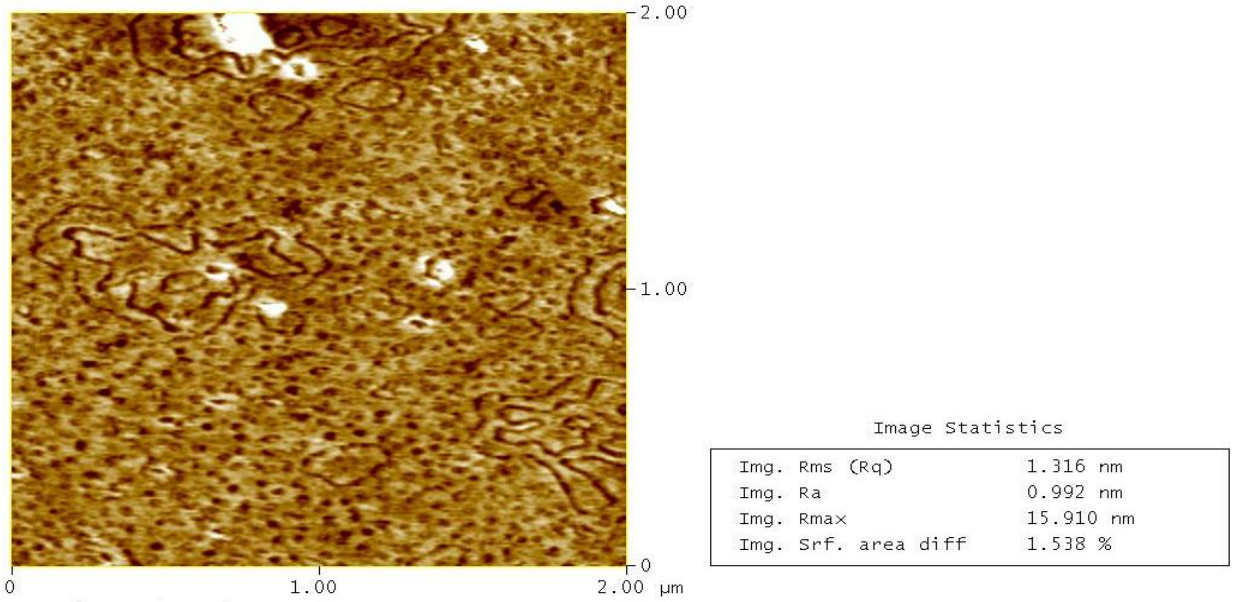

Figure 21: Glass Substrate roughness analysis provided by manufacturer.

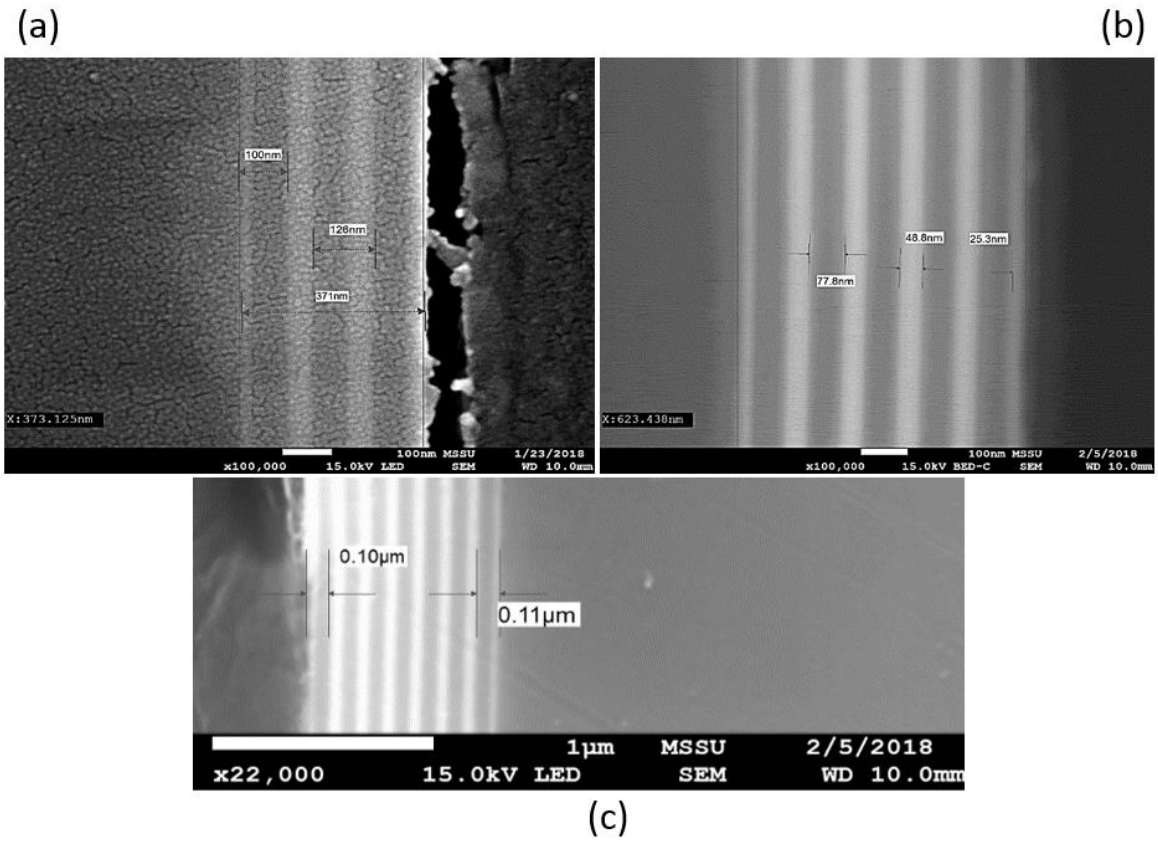

Figure 22: (a) SEM secondary electron image illustrating total thickness and bilayer thickness, (b) Backscattered electron imaging illustrating individual layer thicknesses, (c) Bilayer thickness of the outermost (Nb+Si) layers in stack.

4.2.2.1 Verification of anomaly identified in Multilayer sample

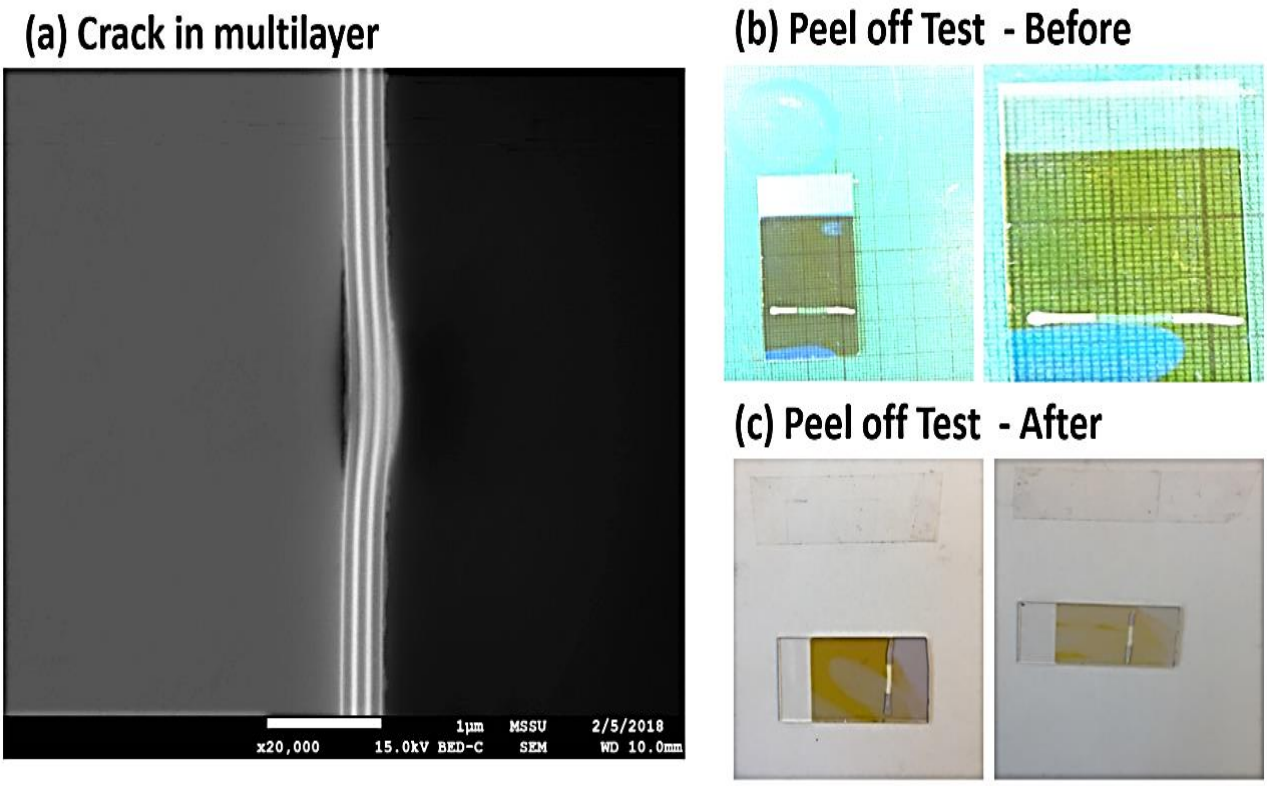

Figure 23: SEM imaging of probable buckling in the in the 7 layer sample

Figure (20a) above is indicative of some form of cracking in one of the multilayer samples observed during SEM imaging. The crack is indicative of Buckling in the structure. However, other sources of the probable cause of the anomaly observed may be; (a) Differences in the rate of wear imposed in the film during sample preparation via metallurgical polishing. The polishing was performed with an abrasive rating consistent to silicon. Consequently, what has been observed is a tear from the substrate, which is indicative of the Niobium layer failing under stress. Other sources of probable causes may be poor adhesion in the multilayers, this theory has been verified and it appears that the films behave well in terms of the adhesive properties since the adhesive tape test conducted revealed little or no failure of the surface coating and is an indication that the films perform well under the effect of shear forces. Figure (20c) shows the minimal amount of coating removed from the 11 and 15 layer samples deposited on glass substrate as the adhesive tapes used were placed on a white background to aid visualization of the level of material which ripped off during the peel off test.

4.2.3 AFM Surface Roughness Analysis

Ex situ AFM was used for the characterization of the surface topography, this was done to verify the suspected evolution with increasing film thickness for the multilayers in the present study. The acquired AFM images have been used to carry out statistical analysis of the surface and important parameters, such as height-height correlation function, correlation length, and thickness exponent of correlation length have been obtained. The root Mean Square Roughness (RMS) was determined at sections taken at five distinct and arbitrary areas on the AFM images. This was done to induce an averaging effect and essentially reduce error due to artefacts. Figures 21 show the AFM micrographs of the 7, 11 and 15-layer samples. The 2D and 3D Images and table 9 shows a comparison of R_{max} for the 7, 11 and 15 layers respectively. The AFM study also shows a progressive increase in average surface RMS with the increase in the number of layers. Notably, the AFM results presented herein are convoluted with information based on the probe tip geometry. This phenomenon is referred to as tip imaging and depending on the size and the geometry of the tip, features may appear to be broader than they are in reality.

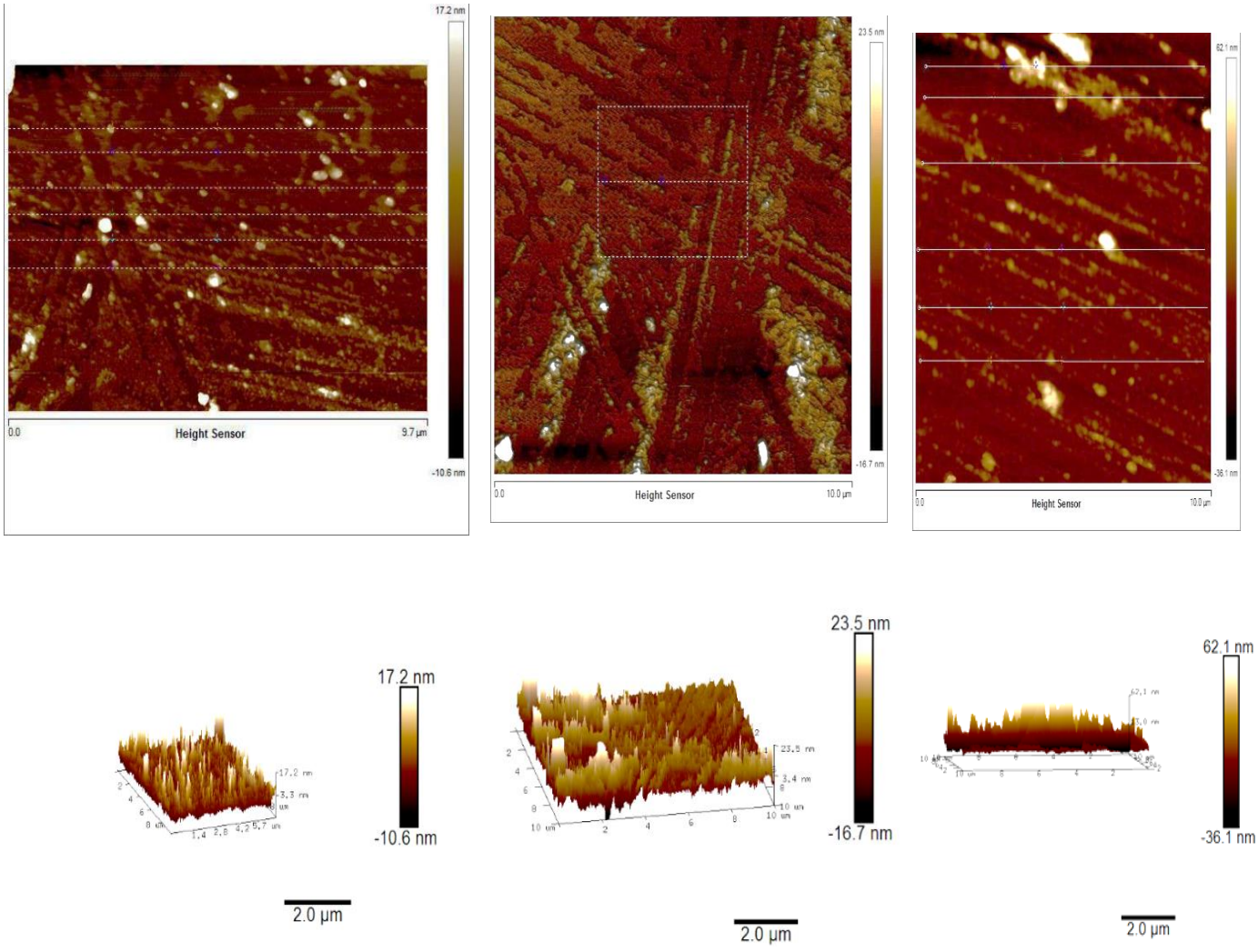

Figure 24: 2D and 3D AFM images of the surface illustrating section cuts and R_{max} progression (7, 11 and 15 layers presented from left to right of the page).

In order to carry out an in-depth data manipulation and analysis from AFM Nasoscope Analysis software, an approach was developed to examine surface topography and characteristics. Due to the fact that each of the data analysis mode considered ("Roughness", "Power Spectral Density", and "Section") provide distinct functional features in terms of surface topographic information, they have all been utilized simultaneously to provide a more valid assessment of the surface topography. The roughness analysis parameters to consider are shown in table 8, the PSD height range indicates the difference between the maximum and minimum heights at the marked location in the AFM images. The mean RMS obtained by section feature aided in examination of the surface topography and the possible existing defects. The image area difference (%) represents the difference between the image's three dimensional footprint areas. The R_{max} indicates the maximum vertical distance between the highest and lowest data points on the multilayer samples and has been illustrated in figure 24.

Table 8: Comparison of AFM roughness analysis for the 7, 11 and 15 layer samples

Multilayer sample number	**Section data**		**Roughness data**				**PSD data**	
	Mean RMS (nm)	*Height Range (nm)*	*Area difference (%)*	*Rq (nm)*	*Ra (nm)*	*Rmax (nm)*	*Equivalent RMS (nm)*	*Total power (µm)^2*
7	1.91	(-3.4 to 9.78)	2.44	4.2	3.01	17.2	1.78	14.9
11	2.21	(-1.50 to 4.90)	1.83	5.5	3.47	23.5	2.09	30.6
15	2.97	(-2.05 to 75.5)	1.41	10.4	5.11	62.1	2.79	103

4.2.4 Surface and interface Correlation Hypothesis

In this section, the results from the analysis performed using the power spectral density analysis tool are utilized in an attempt to demonstrate the dynamic scaling hypothesis in which time and space are considered simultaneously to illustrate oscillatory growth of roughness in the multilayer films. The surface roughness of the 7, 11 and 15 layer films have been plotted as a function of film thickness and deposition time. It is expected from theory that the overall roughness at the interface increases with the number of bilayers and this is confirmed by figure 25 illustrating the effect of bilayer thickness on roughness evolution in growth of multilayers. This plot is in agreement with the trend estimated by the power spectral density analysis tool as summarised in figure 23. However, further analysis is required to verify the validity of this hypothesis. The utility of PSD is that it encompasses statistical information that is unbiased by the scan size and pixel resolution and this method can be methodically applied to reconstruct surface parameters using topography measurements. The graph plotted using manufacturer supplied thicknesses and deposition times and the dynamic scaling theory is shown in figure 23, the plot incorporates estimations for growth exponents obtained from findings by Biswas and Bhattacharyya (2011) to determine the interface width via the power scaling law referenced in the equations table located in the appendix. The surface height distribution as shown in figure (23b) is Gaussian and no asymmetry is observed in the histograms. This may be indicative of a homogeneously rough surface on the 7 layer sample. The bilayer thickness in all the samples examined is 100.5nm and 124.5nm at the edges and the middle of the stack respectively, as such it is expected that the 7, 11 and 15 layer sample all follow the trend that the interface roughness is highest in the region of higher bilayer thickness in the

multilayer. The oscillatory progression in the graph illustrates the periodic roughening and smoothening speculated to occur at the [Nb-Si] and [Si-Nb] interfaces respectively.

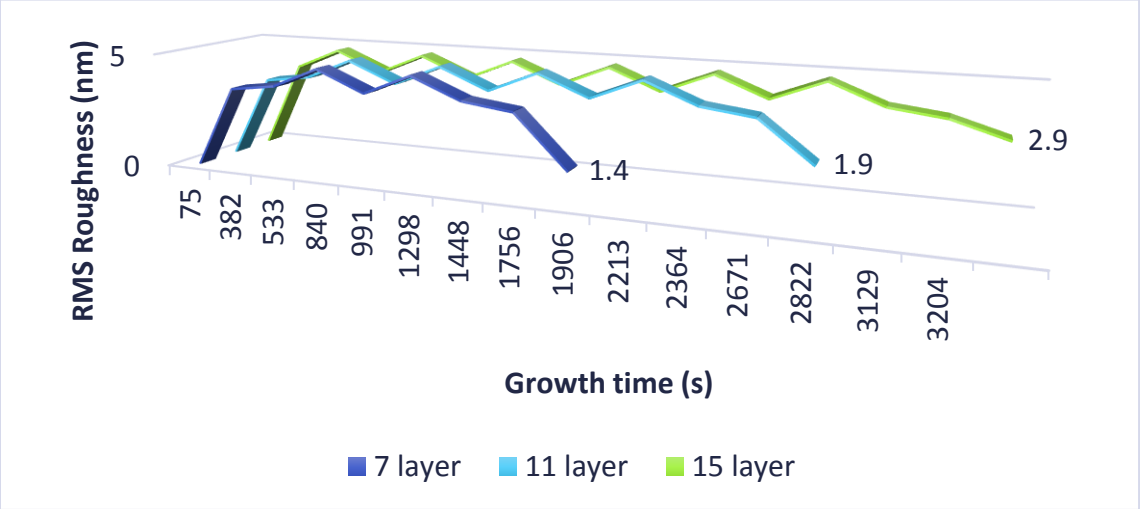

Figure 25: Power law correlation of interface width and bilayer thickness as it relates to roughness evolution from substrate to surface. The plot shows the transition for 7, 11 and 15 layer samples plotted using interface widths calculated by DST and surface roughness measurements from AFM.

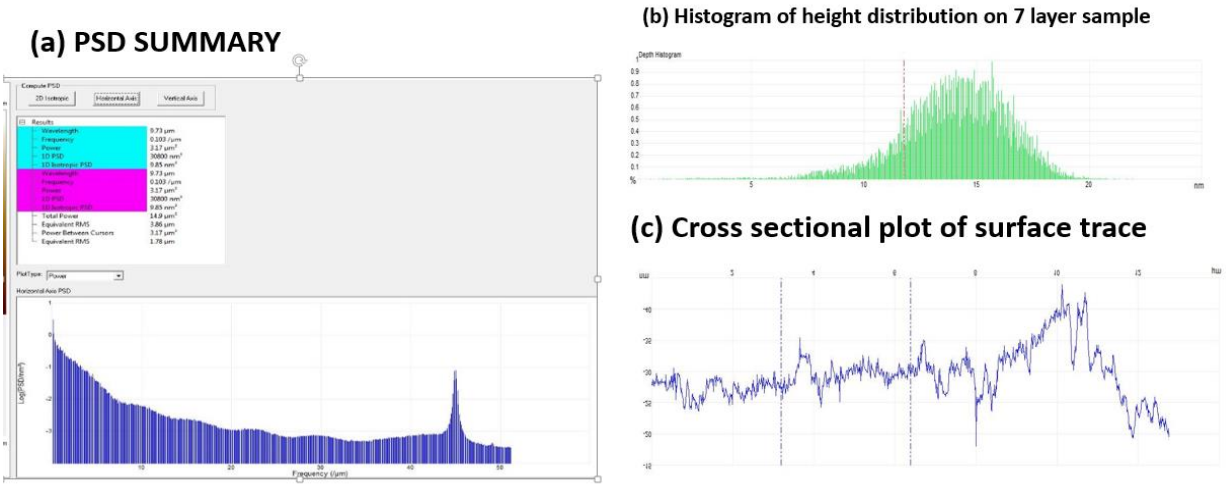

Figure 26: (a) PSD data summary and tapered plot

The tapered PSD plot defines the characteristics of a flat isotropic surface, the spike observed on figure 23 (c) is indicative of the nature of the spacing on the terraces observed by the AFM on the surface of the 7 layer sample, although the complete dynamics of this analysis tool have not been explored by the researcher, the similarities in the PSD and roughness correlation demonstrate similar trends in the shape of the slope for the 7, 11 and 15 layer samples. It is hoped that these trends are further investigated to attain a better quantification of surface and interface roughness parameters.

4.3 Optical Performance Analysis

The optical properties of multilayer films were studied to determine the transmission at the principal wavelength (450 nm) of the multilayer films. These optical measurements helped to verify whether the losses in transmission with the addition of layers was due to unintended diffuse reflection (scatter) which occurs as a result of increasing surface roughness. The terms specular reflectivity refers to conditions of a surface being perfectly reflective (angle of reflection equals angle of incidence). Diffused reflectivity on the other hand refers to scattering of light in all directions, in essence the angle of incidence does not equal angle of reflection

The specular and diffuse measurement spectra shown in figure 24 show that the maximum reflectance achieved was 97.01 % and 97.41 % for the 11 and 15 layers respectively. This high reflectance is due to the constructive interference of the beams and it is facilitated by the phase agreement in reflected beams from multilayer films. This progressive increased was confirmed by theoretical calculations which yielded 96.7% and 99.4 % for the 11 and 15 layer sample respectively. Based on (Ohring, 1995), the magnitude of the reflectance increases with the number of layers. In addition, the number of sideband oscillations outside the high-reflectance zone also increases with number of layers. Cold mirrors are known to have a high reflectivity for visible light and a corresponding high transmission for infrared radiation and this reflected in the reflectance measurements below. The fact there is no absorption is a good indication that the films are stoichiometric. The transmittance spectra presented below are derived from the reflectance spectra. If there was any absorption it would be indicative of free metal within the films and would be indicative of sub-stoichiometric samples. Notably, the expectation from literature is that the multilayers show little or no absorption, as a result findings follows theoretical trends.

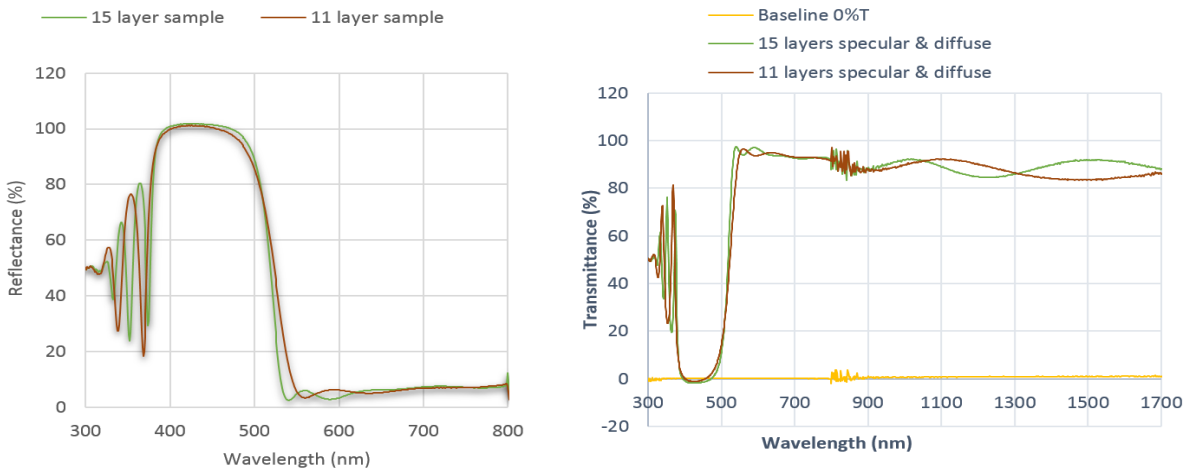

Figure 11: Specular and diffused reflectance and transmittance spectra

The diffuse reflectance yielded a better understanding on the reflected radiant energy that has been partially transmitted and scattered by the surface with no defined angle of reflection. Consequently, the AFM surface roughness values on the 11 and 15 multilayer samples reflect average RMS roughness of 2.1 nm and 2.9 nm respectively and the diffused reflectance spectra indicates a maximum reflectance of 1.9% and 2.1 % within the band gap (high reflectance zone) as shown in figure 24. A bump is observed on the

diffused and the spectra, this is most likely attributed to noise in the systems. Indicating that the instrument has not applied the baseline correction as well as it should have. This may be attributed to the change of grating on the spectrophometer utilised for the measurements.

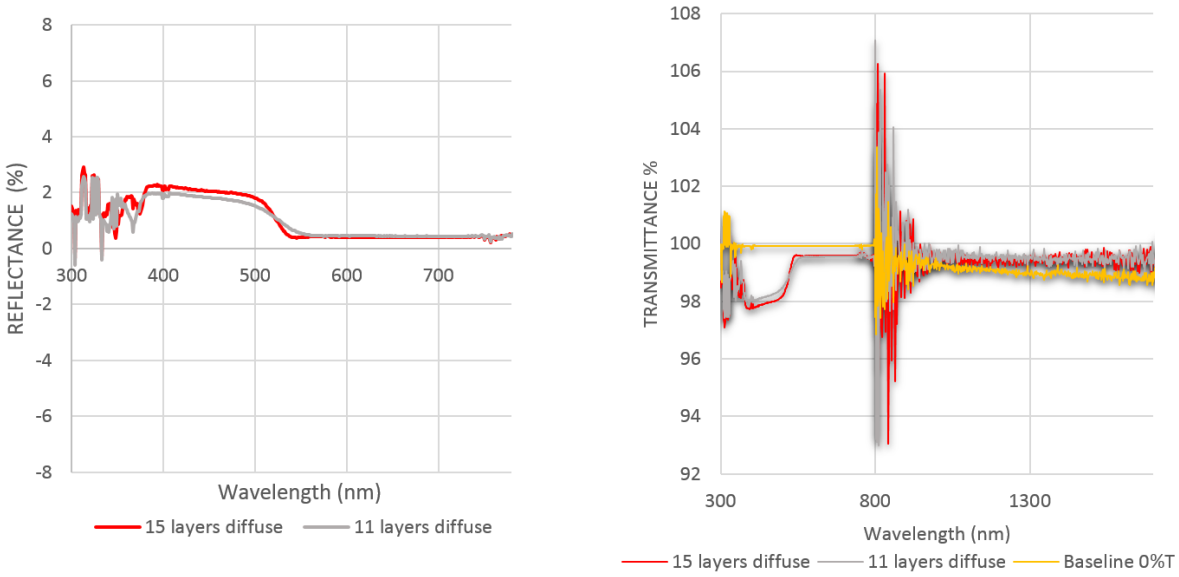

Figure 24: Diffused reflectance spectra for the 11 and 15 layer samples.

5 CONCLUSION

The connection between macroscopic and microscopic properties, and deposition parameters is essentially vital in the process of enhancing dielectric material characteristics for a given application. Depth profiles through multilayer samples comprising of Nb_2O_5 and SiO_2 deposited by a novel technology that utilizes the target efficiently have been characterised. Firstly, significant observations can be made that the surface is significantly depleted with oxygen during the erosion of the niobium pentoxide layer. This effect exists due to the preferential sputter removal of oxygen atoms which can be caused by a number of different factors or a cumulative effect of these mechanisms such as the ion beam energy and the angle of incidence. The observed depletion naturally leads to a reduction of the oxygen removal rate, on the other hand sputter equilibrium conditions are observed in silica layers where the flux of sputtered particles is similar to the original sample composition. Results attained from the experiment have been verified against findings by Hoffman and Sanz as shown in figure 27, where similar work has been performed. It is observed that the oxygen concentration depletion occurs in tandem with Niobium enrichment, the measured atomic concentrations significantly deviate from the bulk oxide sample composition for Nb_2O_5 but only slightly for SiO_2. Therefore, it follows that the level of preferential sputtering observed for the monatomic depth profile is higher in comparison to the Clustered ion beam. Secondly, the interface between the oxide and the metal has been identified from the alternating abrupt decay of Nb layers which is accompanied by a corresponding increase of the Si-signal. Assuming a linear

dependence between ion dose and eroded depth, the 16%-84% decay interval of the oxygen signal was used to deduce an average interface width of 5.49 nm. However, it should be noted that the result attained by this method is susceptible to error caused by artefacts induced by the impinging ions which limit the achievable depth resolution. The HiTUS technology has the capability to control the growth mechanism of the material, ranging from amorphous to crystalline and also directing the preferred crystalline direction (Plasma Quest, 2018). As such the multilayers investigated were expected to be amorphous in nature based on design, the spurious peaks observed in the XRD spectra may be attributed to the presence of filters in the system which introduce discontinuities into the spectrum in diffraction grating based instruments. The XRD spectra closely fitting into trends which exhibit sample transparency error intrinsic to low absorbing samples. It is suspected that this may be the root cause of the peak position and asymmetry errors observed. The SEM cross-sectional image of the 7 layer sample has indicated signs of buckling which is indicative of compressive stress build up in the layer stack, an adhesive test it has not been observed on any of the other samples

The multilayers examined exhibit high performance in the RMS of reflection of visible and transmission of infrared wavelengths of the electromagnetic spectrum. The 7, 11 and 15 layer samples have demonstrated consistent stoichiometry and the minimal absorption observed is indicative of close to bulk composition regardless of thickness of the multilayer stack. Consequently, it follows that the slight dip in transmission observed with the addition of layers is inherent to the design of the multilayers. The diffused reflection spectra show a correlation with surface roughness of the films, this must be further investigated to establish certainty. The interface roughness correlation with surface roughness was aimed at understanding the behaviour of roughness in a multilayer stack. The results presented are a hypothesis investigated to confirm findings by Jain et al. (2003) on amorphous Ta_2O_5 films. The log scale relationship between growth time and thickness explored follows the trend for the periodic multilayers. However, a significant amount of extra data and analysis is required to confirm this hypothesis.

6 FURTHER WORK

Considering the progression of thin film coatings, it can be concluded that understanding the stress generated during thin film production and its implications on roughness evolution is vital to improve reliability and durability of optical coatings such as the dichroic mirror. Work in this project looked into determining whether there is any theoretical rationale that might explain why there is an observed change in roughness at the interface for films manufactured via a Physical Vapour deposition (PVD). Consequently, it has been suggested that using a two stage growth mode also referred to as modulated ion assistance could yield improvements in multilayer systems.

Furthermore, it may prove useful to examine the multilayer samples with X-ray reflectivity, better theoretical models can be defined to explain why roughness might change at the interface and how variation in bi - layer uniformity and thickness ratio may adversely affect the transmission and reflection properties. XRD analysis could be improved by parallel beam optics in the apparatus to account for sample transparency. Lastly, In-situ measurement via ellipsometry could be incorporated to the time-thickness monitor at PQL to facilitate more accurate data that can help explain the uncertainties involved in the evolution or growth of optical coatings.

7 REFERENCES

A. Paul, G. S. Lodha, “Interface roughness correlation due to changing layer period inPt/C multilayers”, Phy. Rev. B, 65 (245416), (2002).

Baer, D., Engelhard, M., Lea, A., Nachimuthu, P., Droubay, T., Kim, J., Lee, B., Mathews, C., Opila, R., Saraf, L., Stickle, W., Wallace, R. and Wright, B. (2010). Comparison of the sputter rates of oxide films relative to the sputter rate of SiO2. *Journal of Vacuum Science & Technology A: Vacuum, Surfaces, and Films*, 28(5), pp.1060-1072.

Beringer, D., Roach, W., Clavero, C., Reece, C. and Lukaszew, R. (2013). Roughness analysis applied to niobium thin films grown on MgO(001) surfaces for superconducting radio frequency Natl. Bur. Stand. (U.S.) Monogr. 25, 18, 61, (1981)

Baker, M. (2017) Engineering Materials. \Lecture notes. University of Surrey.United Kingdom

Biswas, A. and Bhattacharyya, D. (2011). Correlation of interface roughness for ion beam sputter deposited W/Si multilayers. Journal of Applied Physics, 109(8), p.084311.

Briggs, D. and Seah, M. (1988). Practical surface analysis by Auger and X-ray photoelectron spectroscopy. Chichester: Wiley.

Coşkun, Ö. and Demirela,, S. (2013). The optical and structural properties of amorphous Nb2O5 thin films prepared by RF magnetron sputtering. Applied Surface Science, 277, pp.35-39.

Cullity, B. (2015). *Elements of X-ray diffraction*. Utgivningsort okänd: Scholar's Choice.

Ghafoor, N. (2005). Growth and Nano-structural Studies of Metallic Multilayers for X-ray Mirrors. Thin Film Physics Division Department of Physics and Measurement Technology Linköping University, 581 83 Linköping, Sweden, (1193), pp.57-60.

Guo, S., Sushkov, A., Park, D., Drew, H., Kolb, P., Herman, W. and Phaneuf, R. (2014). Impact of interface roughness on the performance of broadband blackbody absorber based on dielectric-metal film multilayers. *Optics Express*, 22(2), p.1952.

Gupta, M., Gupta, A., Phase, D., Chaudhari, S. and Dasannacharya, B. (2003). Development of an ion-beam sputtering system for depositing thin films and multilayers of alloys and compounds. *Applied Surface Science*, 205(1-4), pp.309-322.

Halindintwali, S., Knoesen, D., Swanepoel, R., Julies, B., Arendse, C., Muller, T., Theron, C., Gordijn, A., Bronsveld, P., Rath, J. and Schropp, R. (2010). Synthesis of nanocrystalline silicon thin films using the increase of the deposition pressure in the hot-wire chemical vapour deposition technique. South African Journal of Science, 105(7/8).

Haque, M. and Bhattacharya, D. (2013). Surface roughness and interface width scaling of magnetron sputter deposited Ni/Ti multilayers. *Journal of Applied Physics*, 114(10), p.103508.

Hardee, C. (2018). Confocal Microscopy - Interference Filters for Fluorescence Microscopy. [online] Olympus-lifescience.com. Available at: https://www.olympus-lifescience.com/de/microscope-resource/primer/techniques/confocal/interferencefilters/ [Accessed 14 May 2018].

Heavens, O. (1965). *Optical properties of thin solid films*. New York: Dover.

Hoffman, D. and Thorton, J. (1989). Stress-related effects in thin films. *Thin Solid Films*, 171(1), pp.5-31.

Hofmann, S. (2000). Ultimate depth resolution and profile reconstruction in sputter profiling with AES and SIMS. *Surface and Interface Analysis*, 30(1), pp.228-236.

Instruments, S. (2018). Diffuse Reflectance Measurement. [online] Ssi.shimadzu.com. Available at: https://www.ssi.shimadzu.com/products/uv-vis-spectrophotometers/diffuse-reflectance-measurement.html [Accessed 10 May 2018].

Janicki, V., Sancho-Parramon, J., Yulin, S., Flemming, M. and Chuvilin, A. (2012). Optical and structural properties of Nb2O5–SiO2 mixtures in thin films. *Surface and Coatings Technology*, 206(17), pp.3650-3657.

Jain, P., Juneja, J., Karabacak, T., Rymaszewski, E. and Lu, T. (2002). Surface Roughness Evolution in Amorphous Tantalum Oxide Films Deposited by Pulsed Reactive Sputtering. *MRS Proceedings*, 749.

Kubart, T., Nyberg, T. and Berg, S. (2010). Modelling of low energy ion sputtering from oxide surfaces. Journal of Physics D: Applied Physics, 43(20), p.205204.

Liu, Z. and Shen, Y. (2004). Oscillating growth of surface roughness in multilayer films. *Applied Physics Letters*, 84(25), pp.5121-5123.

Macleod, H. (2010). *Thin-film optical filters*. Boca Raton, FL: CRC Press/Taylor & Francis.

Madsen, C. and Zhao, J. (2001). *Optical filter design and analysis*. Hoboken, NJ: Wiley-Interscience.

Malherbe, J., Hofmann, S. and Sanz, J. (1986). Preferential sputtering of oxides: A comparison of model predictions with experimental data. *Applied Surface Science*, 27(3), pp.355-365.

Moulder, J. and Stickle, W. (2018). *Handbook of X-Ray photoelectron spectroscopy*. 1st ed. United States of America: Physical electronics Inc, 6509 Cloud Drive, Minnesota 55344.

Ohring, M. (1995). *Engineering materials science*. San Diego: Academic Press.

Opticsbalzers.com. (2018). Optics Balzers - Dichroic Mirrors. [online] Available at: https://www.opticsbalzers.com/en/products/mirrors/dichroic-mirrors.html [Accessed 13 May 2018].

Özer, N., Rubin, M. and Lampert, C. (1996). Optical and electrochemical characteristics of niobium oxide films prepared by sol-gel process and magnetron sputtering A comparison. Solar Energy Materials and Solar Cells, 40(4), pp.285-296.

Plasma Quest. (2018). *Photonics & Precision Optics - Plasma Quest*. [online] Available at: https://www.plasmaquest.co.uk/application/photonics-precision-optics/ [Accessed 12 May 2018].

Richter, F., Kupfer, H., Schlott, P., Gessner, T. and Kaufmann, C. (2001). Optical properties and mechanical stress in SiO2/Nb2O5 multilayers. *Thin Solid Films*, 389(1-2), pp.278-283.

Savage, D., Schimke, N., Phang, Y. and Lagally, M. (1992). Interfacial roughness correlation in multilayer films: Influence of total film and individual layer thicknesses. *Journal of Applied Physics*, 71(7), pp.3283-3293.

Schiffmann, K. and Vergöhl, M. (2012). Characterization of 31 nonperiodic layers of alternate SiO2/Nb2O5on glass for optical filters by SIMS, XRR, and ellipsometry. Surface and Interface Analysis, 45(1), pp.490-493.

Smith, W. (2000). Modern optical engineering. New York: McGraw Hill.

Specs.de. (2018). [online] Available at: http://specs.de/cms/upload/PDFs/IQE11-35/sputter-info.pdf [Accessed 10 Apr. 2018].

Sultan Z, M. and N, S. (2015). Analysis of Reflectance and Transmittance Characteristics of Optical Thin Film for Various Film Materials, Thicknesses and Substrates. Journal of Electrical & Electronic Systems, 04(03).

Swanson, Fuyat., Natl. Bur. Stand. (U.S.), Circ. 539, 3, 24, (1954).

Viana, M., Mohallem, T., Nascimento, G. and Mohallem, N. (2006). Nanocrystalline titanium oxide thin films prepared by sol-gel process. Brazilian Journal of Physics, 36(3b), pp.1081-1083.

Wasa, K. and Hayakawa, S. (1992). Handbook of sputter deposition technology. Park Ridge, N.J., U.S.A.: Noyes Publications.

Watts, J. and Wolstenholme, J. (2008). *An introduction to surface analysis by XPS and AES*. New York: Wiley.

Whiteside, P., Chininis, J. and Hunt, H. (2016). Techniques and Challenges for Characterizing Metal Thin Films with Applications in Photonics. Coatings, 6(3), p.35.
Widjonarko, N. (2016). Introduction to Advanced X-ray Diffraction Techniques for Polymeric Thin Films. Coatings, 6(4), p.54.

Windt, D., Christensen, F., Craig, W., Hailey, C., Harrison, F., Jimenez-Garate, M., Kalyanaraman, R. and Mao, P. (2000). Growth, structure, and performance of depth-graded W/Si multilayers for hard x-ray optics. *Journal of Applied Physics*, 88(1), pp.460-470.

Wucher, A. (1998). Surface and Thin Film Analysis with Electron and Mass Spectrometric Techniques. *Materials Science Forum*, 287-288, pp.61-86.

Xiaoming, J. and Ziqin, W. (1991). Bragg's Law with Refractive Correction of Low-angle x-ray Diffraction for Periodic Multilayers. *Chinese Physics Letters*, 8(7), pp.356-359.

Xpssimplified.com. (2018). *XPS Depth Profiling*. [online] Available at: https://xpssimplified.com/depth_profiling.php [Accessed 5 Apr. 2018].

8 APPENDIX

Table 9: Scaling parameters derived from (Haque, M. and Bhattacharya, D. (2013), extrapolated results indicated in green.

Element	Beta	Alpha	Atomic Number	Atomic mass
Fe	0.22	0.79	26	55.8
Mo	0.42	0.89	42	95.5
Pt	0.26	0.9	78	195.08
Ni	0.57	0.9	28	58.6
Ti	0.42	0.73	22	47.6
Nb	0.4	0.86	41	92.09
Si	0.31	0.625	16	28

Table 10: Supporting equations used for analysis

EQUATIONS USED FOR RESULT ANALYSIS		
XPS compositional analysis	$[(\frac{Xm}{Xo})^s/((\frac{Xm}{Xo})^b]_{calc}$	(Hoffman and Sanz, 1988)
AFM – Dynamic scaling theory	$W = t^{\beta}$	(Haque, M. and Bhattacharya, D. (2013)
Optical Reflectivity	$R_{\lambda/4} = (n_H - n_L n_2)/(n_H + n_L n_2)$	(Ohring, M. (1995)

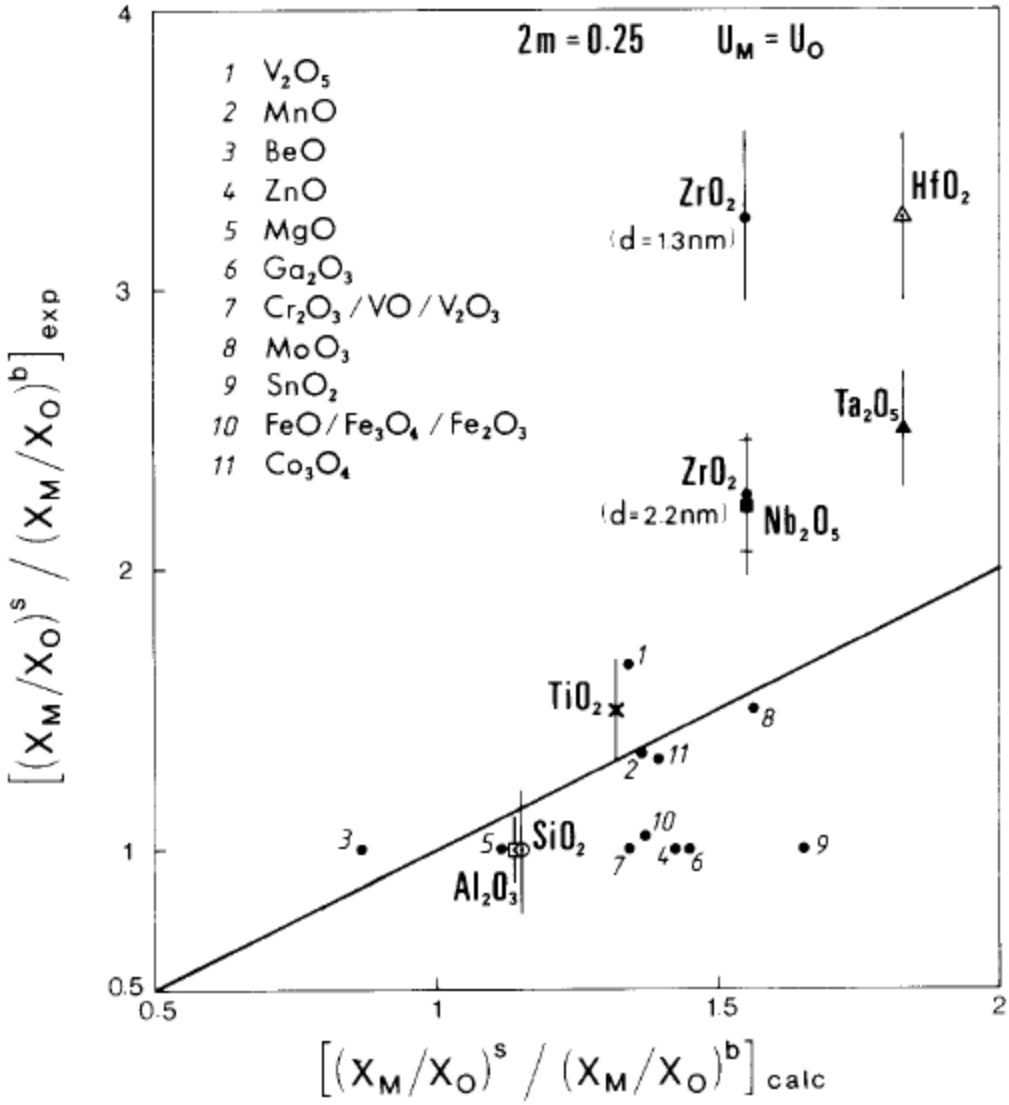

Figure 27: The experimentally determined surface composition ratios of the altered sputtered layers (Hoffman and Sanz, 1986).